

## **ACKNOWLEDGEMENT**

I would like to thank all the Monolith team for their help and guidance of this master thesis, especially to Ing. Marek Václavík for his assistance while writing thesis and Richard Knopp for his help at experimental work.

My biggest THANK YOU belongs to my family for their support, patient and encouraging in all my life. Also huge thank you belongs to my girlfriend for her support in every area of my study and personal life.

## **SOUHRN**

V dnešní době má každé auto se spalovacím motorem ve výfukovém potrubí umístěn katalytický konvertor, který snižuje množství škodlivin vznikajících nedokonalým hořením paliva. Katalytické monolitické konvertory plynných emisí mají voštinovou strukturu s velkým počtem otevřených kanálků, na nichž je nanesená porézní katalytická vrstva. Pro zachycení pevných částic (sazí) se používá filtr, který je součástí systému pro ošetření spalin. Kanálky filtru jsou střídavě zaslepeny na vstupním či výstupním konci, takže plyn musí prostoupit přes porézní stěnu do sousedního kanálku, a tím se saze odfiltrují. Aby byl celý systém kompaktnější, může být katalytický materiál nanesen přímo do filtru – takové zařízení se nazývá katalytický filtr. U všech filtračních systémů je významným parametrem tlaková ztráta.

Tato práce je zaměřena na vývoj podtlakového nanášení porézní katalytické vrstvy na monolitický keramický filtr a nalezení vhodných parametrů pro nanesení tenkých vrstev tvořených  $\gamma$ -Al<sub>2</sub>O<sub>3</sub>. Byl zkoumán vliv pH (viskozity) suspenze, velikosti částic, hodnoty podtlaku a předchozího namočení substrátu na délku a tloušťku nanesené vrstvy. Připravené vzorky byly analyzovány rastrovacím elektronovým mikroskopem. Pro sadu finálních vzorků, které byly naneseny z obou dvou stran, byla změřena tlaková ztráta při průtoku plynného dusíku. Bylo otestováno několik různých způsobů nanesení porézní vrstvy a vyhodnocen jejich vliv na výslednou tlakovou ztrátu filtru.

## SUMMARY

Nowadays, a catalytical converter is implemented in exhaust pipes of every car with internal combustion engine to reduce the amount of pollutants produced during an unideal burning of fuel. Catalytical converters of gaseous emissions have a honeycomb structure with high number of open channels coated with porous catalytic layer (flow-through design). Particulate matter (soot) is trapped in a particulate filter which is also placed in the exhaust gas aftertreatment system. Filter channels are alternately plugged at one end so that the exhaust gas has to permeate through porous walls to an adjacent channel and the soot is filtered out. To make the system more compact, catalytic material can be coated directly on filter walls – such a device is then called a catalytic filter. Pressure loss is a significant parameter for all filter systems.

This master thesis is focused on developing a vacuum-coating procedure of ceramic filter substrate and finding suitable parameters for deposition of a thin  $\gamma\text{-Al}_2\text{O}_3$  layer formed. Particularly, it was investigated how the suspension pH (viscosity), particle sizes, vacuum level and wetting the substrate prior to the coating affect the resulting coated length and layer thickness. The prepared samples were analyzed by scanning electron microscopy. Set of final samples was coated from both sides of the filter substrate and tested under flow of nitrogen for pressure drop. It was investigated how the varied coating conditions influence the filter pressure loss.

# CONTENTS

1	INTRODUCTION.....	1
2	LITERATURE REVIEW.....	2
2.1	History of Emission Regulations and Automotive Converters Development .....	2
2.2	Emission Formation During Combustion.....	4
2.2.1	Particulate Matter Formation in Petrol Engines .....	6
2.2.2	Particulate Matter Formation in Diesel Engines.....	7
2.3	Structure of Catalytic Converter.....	8
2.3.1	Structure Type of Catalytic Converter.....	9
2.3.2	Particulate Filter .....	12
2.4	Preparation and Coating of Catalytic Layer .....	18
2.4.1	Washcoating .....	19
2.4.2	Properties of $\gamma$ -Al <sub>2</sub> O <sub>3</sub> Particles.....	20
3	EXPERIMENTAL PART .....	21
3.1	Preparation and Characterization of Aqueous Suspension.....	22
3.2	Coating of Monolithic Filter.....	26
3.2.1	Cuboidal Samples .....	27
3.2.2	Cylindrical Samples.....	29
3.3	Pressure Loss of Filters.....	32
3.4	Analysis of Coated Samples .....	33
4	RESULTS AND DISSCUSSION .....	35
4.1	Dip-coating of Cuboidal Samples.....	35
4.2	Vacuum Coating of Cylindrical Samples .....	38
4.2.1	Suspension Loading.....	38
4.2.2	Suspension pH .....	39
4.2.3	Pressure During Vacuum Coating .....	42

4.2.4	Particle Size .....	43
4.2.5	Wet Sample Coating.....	48
4.2.6	Impact of Sealing During Vacuum Coating .....	51
4.3	Testing of Coated Samples .....	52
5	CONCLUSION .....	56
	LITERATURE.....	58
	LIST OF ABBREVIATIONS.....	61
	LIST OF SYMBOLS.....	62
	LIST OF TABLES.....	63
	LIST OF FIGURES .....	64
	APPENDIX.....	67

# 1 INTRODUCTION

Since the 1970s, the numbers of cars is increasing which leads to worse atmosphere in larger cities – Diesel and petrol engines produced a large amount of emissions. The emissions are formed due to unideal combustion of fuel, poor mixing fuel and air in combustion chamber and other effects – carbon oxides, unburned hydrocarbons, nitrogen oxides and particulate matter (soot) are released as a result.

Exhaust gases are treated by catalytic converters – each type of engines has a special system but all use monolithic converter with honeycomb structure. Emissions started to be regulated by “Euro Emissions Standard” developed by European Union for Europe. Since Euro 5, particulate matter is strictly reduced which can only be achieved by installing a particulate filter in the system treating exhaust gases. The monolithic particulate matter filter has the same shape as catalytic converter – catalytic converters are flow-through while filter channels are plugged at one end (gas has to permeate through the porous walls). Generally, converter contains from many small channels, their diameter is approx. 1 mm and length 10 – 15 cm. The catalyst is applied either as a thin layer on the channel walls or inside the porous walls of the filter. Soot is captured and periodically burned by increased temperature of exhaust gases when filter is full of particles. The purpose of the catalyzed particulate filter is to achieve the high filtration efficiency, conversion of pollutants while having low enough pressure loss and large soot storage capacity.

This master thesis was focused to develop vacuum-coating procedure of cylindrical filter samples (same length as industrial filters) and measure their pressure loss. Further research will aim to adding catalytically active metals to  $\text{Al}_2\text{O}_3$  layer and then catalyst activity will be studied in a tubular reactor. Several parameters were observed which influencing coating procedure and layer thickness, such as particle size, viscosity of suspension, vacuum set-up, effect of wetting the substrate with water prior to the coating. When suitable parameters were found, samples were coated from both sides and pressure loss was testing to mimic engine gas flow.

## **2 LITERATURE REVIEW**

In the end of nineteenth century the automobile industry started to produce passenger cars which began to be widely used mainly in large cities and their numbers increased. Harmful components are formed due to unideal combustion of petrol and diesel in the engines, which led to worse air quality in cities.

### **2.1 History of Emission Regulations and Automotive Converters Development**

In the early 1950s, professor Haagen-Smith from California Institute of Technology proved that a part of hydrocarbons and nitrogen oxides, which were part of exhaust gases, reacts in the presence of sunlight. They create oxidants including ozone which has negative impact on human health.<sup>1</sup>

Since the 1970s, research of automotive converters has been conducted with the aim to prepare catalysts with the largest interphase area, lowest pressure drop and long-life durability. The best solution was the monolithic converter with many channels covered with catalytically active layer, which could fulfil the first exhaust gases regulations. The amount of harmful components in exhaust gases in 1975 was reduced 90 %. The emission regulations become constantly stricter and new options need to be found to control amount of emissions.<sup>2, 3, 4, 5</sup>

In Europe the European Union started to improve air quality by “Euro Emissions Standard” (EES) since 1992. In the **Table 1** the development of EES for Diesel and petrol engines is shown.<sup>5</sup> It can be seen that particulate matter (also PM, or soot) limit is reduced since Euro 1, first by mass (g/km) and only for Diesel engines. The number of particulates became limited as the last of all components. Particulate matter has been limited since 2009 also for petrol motors with direct fuel injection (GDI engines).<sup>5</sup> The reason for PM formation is described below in subchapters “Particulate Matter Formation in Petrol/Diesel Engines”.

**Table 1** – Development of European Emission Standard for passenger automobiles (category M1).<sup>6</sup>

Emission Norm	Validation Date	CO [g/km]	HC [g/km]	NO <sub>x</sub> [g/km]	HC + NO <sub>x</sub> [g/km]	Particulate Matter [g/km]	Number of Particulate Matter per km
<b>For Diesel Engines</b>							
<b>Euro 1</b>	01.07.1992	2.72	-	-	0.97	0.14	-
<b>Euro 2</b>	01.01.1996	1	-	-	0.7	0.08	-
<b>Euro 3</b>	01.01.2000	0.64	-	0.5	0.56	0.05	-
<b>Euro 4</b>	01.01.2005	0.5	-	0.25	0.3	0.025	-
<b>Euro 5a</b>	01.09.2009	0.5	-	0.18	0.23	0.005	-
<b>Euro 5b</b>	01.09.2011	0.5	-	0.18	0.23	0.005	$6 \cdot 10^{11}$
<b>Euro 6</b>	01.09.2014	0.5	-	0.08	0.17	0.005	$6 \cdot 10^{11}$
<b>For Petrol Engines</b>							
<b>Euro 1</b>	01.07.1992	2.72	-	-	0.97	-	-
<b>Euro 2</b>	01.01.1996	2.2	-	-	0.5	-	-
<b>Euro 3</b>	01.01.2000	2.3	0.2	0.15	-	-	-
<b>Euro 4</b>	01.01.2005	1	0.1	0.08	-	-	-
<b>Euro 5</b>	01.09.2009	1	0.1	0.06	-	0.005	-
<b>Euro 6</b>	01.09.2014	1	0.1	0.06	-	0.005	$6 \cdot 10^{11}$

## 2.2 Emission Formation During Combustion

Output of exhaust gases from combustion engine contains both gaseous harmful components and particulate matter. Nowadays gaseous emissions regulations are aimed at carbon monoxide (CO), unburned hydrocarbons (HC) and nitrogen oxides (NO<sub>x</sub>). Based on assumption that the mixture of fuel and air is stoichiometric (combustion process is considered as ideal), the products would be water and carbon dioxide, see equation (1). In reality, the Diesel engine there is air in excess to fuel and the control unit of petrol engine sets the mixture close to stoichiometric, however, the combustion is not ideal in either case. Example of real exhaust composition for petrol engine is shown in the **Table 2** (composition is in volume or molar percentages)<sup>7</sup>:

**Table 2** – Example of real exhaust gases composition.<sup>7</sup>

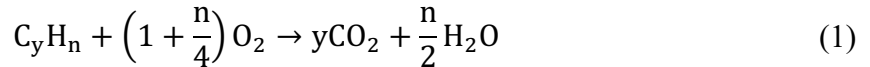
Components	Amount
<b>Water</b>	10 %
<b>Carbon oxide</b>	0.5 %
<b>Carbon dioxide</b>	10 %
<b>Oxygen</b>	0.5 %
<b>Nitrogen oxides (NO<sub>x</sub>)</b>	900 ppm
<b>Hydrogen</b>	0.17 %
<b>Unburned hydrocarbons (HC)</b>	250 ppm

Emissions of unburned hydrocarbons and carbon oxide are also formed due to effect of cold wall strokes of engines. Cold start of engine cause higher fuel consumption, emissions and mechanical abrasion. Also engine works under rich conditions to heat up whole system (engine, catalytic converters, etc.).

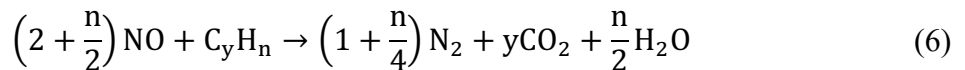
In catalytic converter they react with oxygen forming harmless components, see equation (1) and (2). If the oxygen is not presented the carbon monoxide reacts with

water steam, see equation (3). Around the spark plugs and at higher temperatures ( $> 1500$  °C) during combustion the nitrogen with oxygen forms nitric oxide and nitrogen dioxide – marked as  $\text{NO}_x$ . They are reduced by carbon monoxide, hydrogen or by unburned hydrocarbons, see equation (4), (5) and (6).

Oxidation of unburned hydrocarbons and carbon monoxide:



Reduction of nitrogen oxides (equations mentioned for NO only, they are analogous for  $\text{NO}_2$ ):



These reactions need a specific temperature to be ignited so high conversion is obtained which is a problem right after the engine is started – the catalytic converter is cold and the conversions are low. When the catalytic converter is placed near to the end of tailpipe, it needs many minutes to be heated up. To solve this problem a small catalytic converter can be added right behind the engine and it is warmed faster.<sup>7</sup>

### 2.2.1 Particulate Matter Formation in Petrol Engines

Port fuel injection (PFI) engines in passenger cars have been replaced by gasoline direct injection (GDI) engines because of their greater power output, lower fuel consumption and higher thermal efficiency. The main difference is that GDI engines directly inject fuel into the combustion chamber and the whole process (evaporation and mixing) is much shorter than PFI engines. Also particles contain more soot and lower organic components for GDI engines. Particulate matter can be formed by two reasons:

- Fuel can be sprayed on the engine surface (piston, valve, cylinder wall) where fuel droplets can adsorb on that surface;
- Fuel-rich regions can be created by insufficient mixing of fuel and air;
- Incomplete oxidation of fuel.<sup>8</sup>

During combustion procedure most of particulate matters are oxidized into CO<sub>2</sub> and intermediates.<sup>8</sup>

Particulate matters (or particles) are mainly created from unburned fuel and they are called soot. Soot is formed from fuel-rich regions under high pressure – gas phase (and partially liquid phase) is changeover to solid phase. This process is called nucleation mode. Whole procedure of forming soot particles consists of six processes which are illustrated in the **Figure 1**:

- Pyrolysis;
- Nucleation;
- Coalescence;
- Surface growth;
- Agglomeration;
- Oxidation.<sup>8</sup>

Fuel is decomposed and produces gas phase precursors or soot during pyrolysis process. Polycyclic aromatic hydrocarbons (PAHs) can be the key intermediates in soot generation. The most crucial process of particle formation is to form first aromatic ring which grows to create PAHs – they do not have to be present in the fuel. PAHs can be

created from small aliphatics (acetylene, propyne,...). Nucleation is procedure in which small particles are generated from organic components. During aggregation process particles assemblage and stick together to create larger particles. Intermediates are oxidized to soot particles at high temperatures.<sup>8</sup>

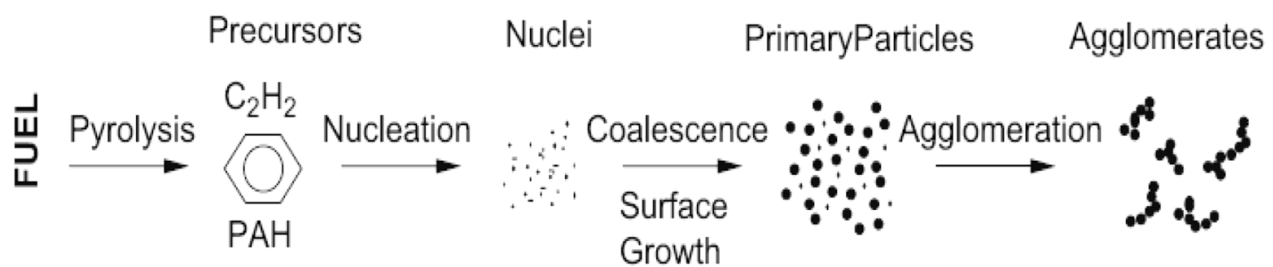


**Figure 1** – Development of particulate matter from fuel.<sup>8</sup>

### 2.2.2 Particulate Matter Formation in Diesel Engines

The principle of particulate matter formation is the same as it is described in subchapter above. As it is shown in the **Table 1**, particulate matter limit has been reduced since Euro 1. Diesel engine is generally more effective than petrol engine, however, it produces larger amount of soot. The inlet, which enters into the stroke where it is compressed and ignited, is more homogenous and the mixture of fuel and gas is stoichiometric in the case of petrol engine.<sup>9</sup> The principle of Diesel engine is different – the air is in surplus and compressed, temperature is increased and fuel is injected into the stroke and combusts spontaneously. However, there can be a heterogenous mixture of fuel-rich regions which are perfect candidate for soot formation.<sup>9</sup>

## 2.3 Structure of Catalytic Converter

Automotive catalytic converter is a device where harmful components react to harmless products. It is located in outlet of the engine exhaust pipe. It consists of porous structure, support and active metals. The most important components are active metals (e.g. Pd, Pt, Rh, Ba, Ce and others) which decrease activation energies of reactions. To obtain high conversions of above mentioned reactions it is crucial to distribute active metals on the support so they have high surface area and so the mass transfer of reactants and products is not limited.<sup>10</sup> Other requirements for catalytic converter are:

- Low pressure drop;
- Chemical stability;
- Thermal stability;
- Mechanical stability;
- Weight;
- Shape;
- Price.<sup>11</sup>

A cylindrical monolithic catalytic converter of monolithic type is shown in **Figure 2**. It has honeycomb arrangement with many small channels which are covered with so-called “washcoat” – a thin layer of support (typically  $\gamma\text{-Al}_2\text{O}_3$ ) containing catalytically active metals. The most valuable advantage of the support is its high interface area and porosity. The pore size is crucial for gas transfer. The IUPAC (International Union of Pure and Applied Chemistry) divides pores due to the size – macropore (bigger than 50 nm), mesopore (2 to 50 nm) and micropore (less than 2 nm);  $\gamma\text{-Al}_2\text{O}_3$  is mesoporous.<sup>12</sup>

The whole process of gas transport can be divided into several steps. Firstly the gas reactants have to be transferred from gas bulk to the particles surface of catalyst particle which is driven by fast volume diffusion. By next step reactants must get to the active center of particle by Knudsen’s diffusion.<sup>11, 13</sup> When they are inside it is needed to be adsorbed by chemisorption, reactions obtained. Products have to be desorbed and then they are transported by same way but in opposite row.

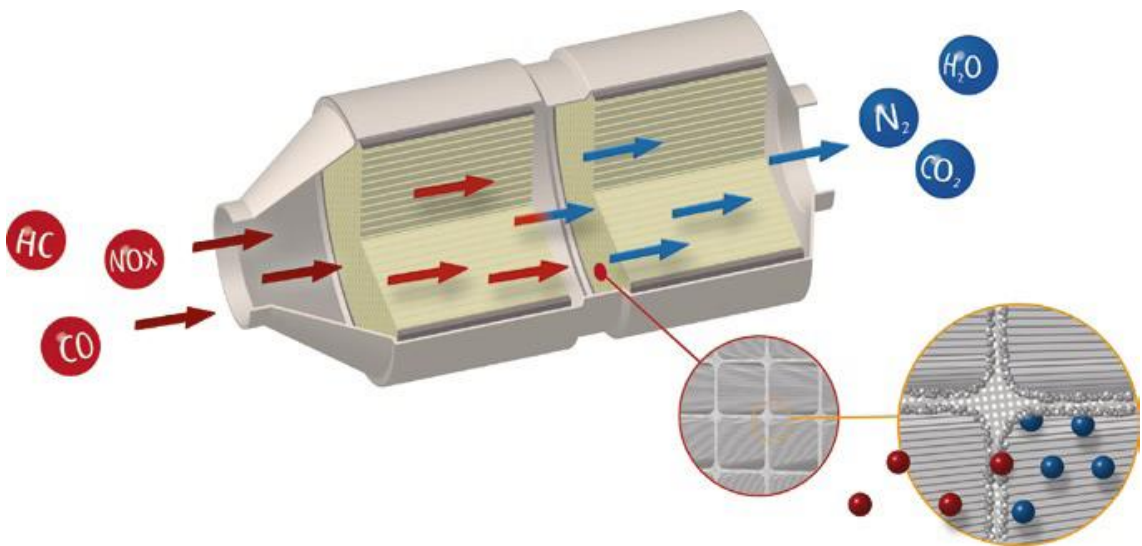


**Figure 2 – Catalytic converter of monolithic type.<sup>14</sup>**

### 2.3.1 Structure Type of Catalytic Converter

Flow-through automotive converters can be divided according to the engine type and their function:

1. Diesel engine
  - a. DOC (Diesel Oxidation Catalyst)
  - b. deNO<sub>x</sub> Technology
    - i. SCR (Selective Catalyst Reduction)
    - ii. NSRC (NO<sub>x</sub> Storage and Reduction Catalyst) (=LNT)
2. Petrol engine
  - a. TWC (Three-Way Catalyst)
  - b. NSCR (NO<sub>x</sub> Storage and Reduction Catalyst) (=LNT)

#### *Diesel Oxidation Catalyst*

The catalyst composition is optimized with regards to the catalysts activity under lean conditions and costs, but their most important components are noble metals (Pt and Pd) impregnated to porous alumina. Their function is to oxidize unburned hydrocarbons (HC) and carbon monoxide (CO) as well as soluble organic fraction (SOF) portion of

PM. They also convert nitric oxide (NO) to nitrogen dioxide (NO<sub>2</sub>). Generally, oxidation reactions release reaction heat which is used for the DPF (Diesel Particulate Filter) active regeneration cycle.<sup>9</sup>

#### *deNO<sub>x</sub> Technology*

NO<sub>x</sub> have to be reduced to nitrogen which cannot be done under lean conditions in the Diesel engine (and some petrol engines as well) because oxygen is in great excess to the fuel. To solve the NO<sub>x</sub> problem, a part of exhaust gases can be recirculated back to engine intake. Using only this option does not fulfill the EES requirements for both NO<sub>x</sub> and PM emission.<sup>14</sup>

Nitrogen oxides might be removed by two options. The first method is to use SCR (Selective Catalytic Reduction) catalyst with ammonia as a reducing agent, which is used for Diesel engines. Ammonia has to be produced in exhaust pipe system by decomposition of urea solution. NH<sub>3</sub> then reacts with NO<sub>2</sub> resp. NO creating N<sub>2</sub> and water. The highest NO<sub>x</sub> conversion can be reached when the ratio of NO/NO<sub>2</sub> concentrations is 1, DOC located in front of the SCR therefore enhances the reactions in the SCR.<sup>15</sup>

LNT (lean NO<sub>x</sub> trap) also known as NSRC is another reduction method of NO<sub>x</sub> which is used for Diesel and petrol engines (in lean conditions<sup>16</sup>). The principle of its function is switching between lean (air surplus) and rich (fuel surplus) conditions. In lean conditions NO<sub>x</sub> are storaged by chemisorption on the surface of catalyst oxides and CO and HC are oxidized during this process. This procedure takes several minutes. When the storage capacity is fulfilled, the engine switches to rich conditions where NO<sub>x</sub> are reduced by unburned CO and HC contained in exhaust gases. Rich procedure takes a few seconds.<sup>17</sup>

#### *Three-Way Catalyst*

TWC is nowadays the most efficient technology for controlling automotive emissions of petrol engines. It is capable of converting all harmful components – CO, HC and NO<sub>x</sub>. The first automobiles with TWC were introduced by Volvo company 1979.<sup>18</sup> This catalytic converter can only work if the mixture fuel-air is stoichiometric, carburetor

therefore had to be replaced by electronically controlled fuel injection. In PFI or GDI an oxygen sensor is placed in the exhaust tube and sends data to microprocessor in the engine control unit, which controls the fuel injection.<sup>4, 19</sup> Based on this system, an exact stoichiometric fuel-air ratio can be achieved (weight ratio is 14.7 which means 14.7 kg of air is needed per 1 kg fuel). The fuel-air ratio during real riding cycle oscillates around this value in a so called “Operating Window”<sup>20, 21</sup>

The oscillations impact the conversion as well. To improve the conversion the catalytic converter contains CeO<sub>2</sub> which can change the oxidation number (from CeO<sub>2</sub> to Ce<sub>2</sub>O<sub>3</sub>) dependence on CO and HC concentrations and store oxygen.<sup>22</sup> CeO<sub>2</sub> has another important function – it stabilizes the  $\gamma$ -Al<sub>2</sub>O<sub>3</sub> which could change the crystalline form to  $\alpha$ -phase. Furthermore it supports the activity of active metals and inhibits the sintering effect of active metals (Pt and Rh).<sup>19</sup>

The **Figure 3** illustrates conversion of NO<sub>x</sub>, CO and HC dependence on fuel-air ratio (marked as  $\lambda$ ) in rich and lean conditions. When the mixture is stoichiometric ( $\lambda = 1$ ) with the mentioned error, the area bordered by dash curve is the Operating Window. In the lean conditions (air is at surplus) the CO and HC are oxidized to CO<sub>2</sub> and there is not enough CO to reduced NO<sub>x</sub> – engine generates too much NO<sub>x</sub>. In the rich conditions (fuel is at surplus) NO<sub>x</sub> are reduced by excess of CO and HC are not converted.<sup>18</sup>

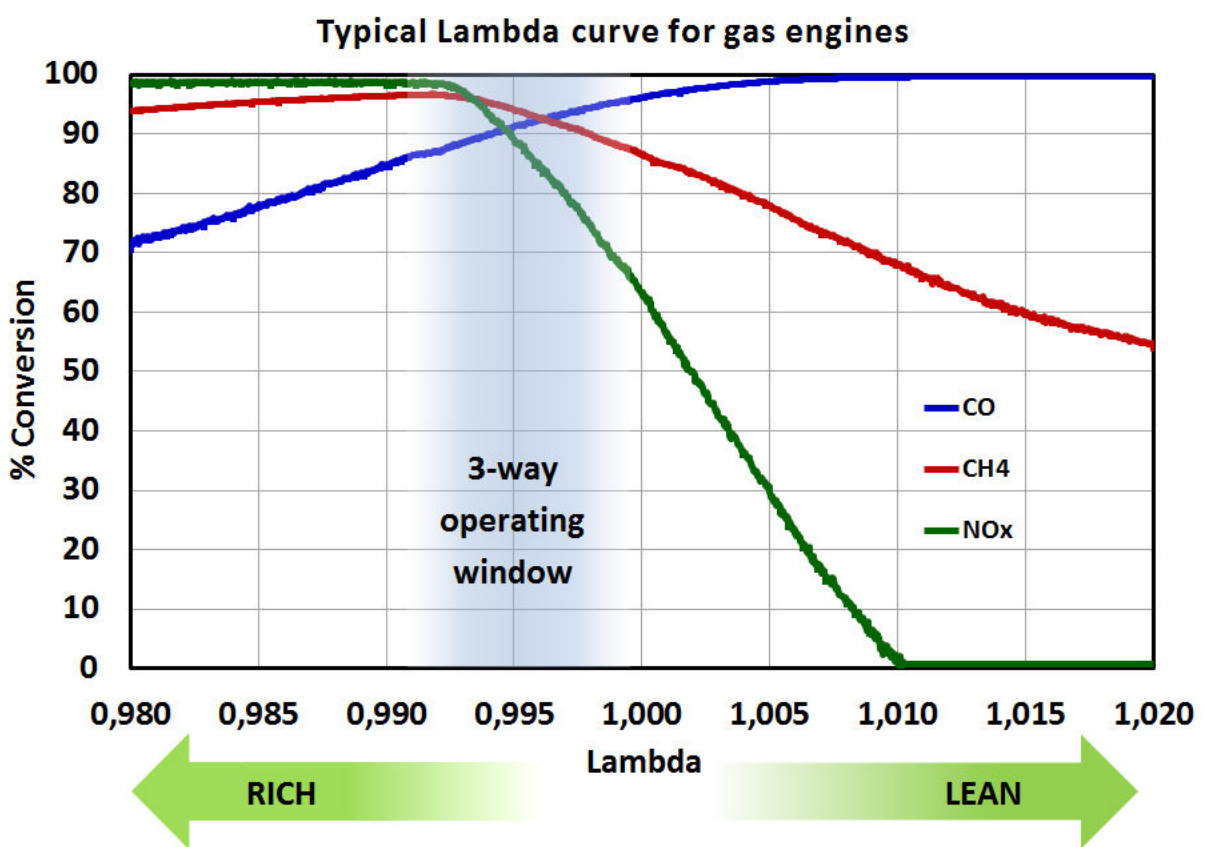


**Figure 3 – Operating Window.<sup>23</sup>**

### 2.3.2 Particulate Filter

Diesel and newly petrol engines have to be equipped with particulate filters to meet emission limits (GPF for petrol engines, DPF for Diesel engines). The monolithic particulate matter filter has the same cylindrical shape as catalytic converter. The main difference is that catalytic converters are flow-through while filter channels are plugged at one end – the exhaust gas has to permeate through the porous walls. The particles are captured on the walls as sketched in the **Figure 4**.<sup>24</sup>

As mentioned above, multiple catalytic converters often need to be combined (one for CO and HC oxidation and other for NO<sub>x</sub> reduction)<sup>25</sup> – aftertreatment system is space-demanding. There are two options – one is to create the catalytically active material in

several layers on a substrate<sup>26, 27</sup>, or directly into the porous substrate of particulate filter<sup>28</sup>. There are some parameters (such as activity of the catalyst, filtration efficiency and pressure loss) which has to be optimized<sup>28</sup>.

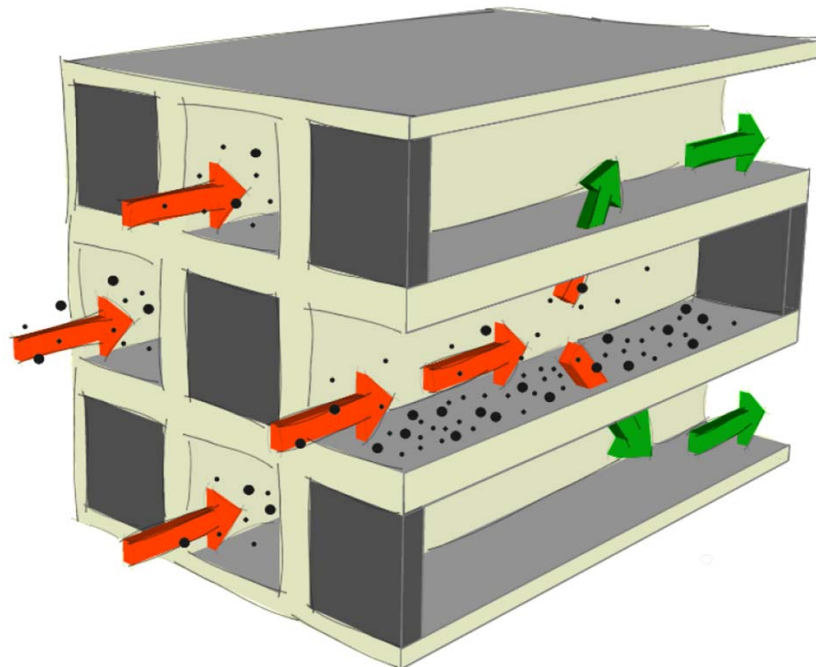


**Figure 4** – The sketch of wall-flow monolithic particulate matter filter.<sup>24</sup>

The regeneration cycle of filter is shown in the **Figure 5**. Generally, when filter contains a significant soot layer (illustrated by “A” part), more fuel is dosed into engine to increase the outlet temperature which helps to burn the soot layer – regeneration of the filter (represented by “B” part). When a layer of oxidation catalyst is applied in the filter the regeneration can be provided at lower temperature<sup>9, 29</sup>.

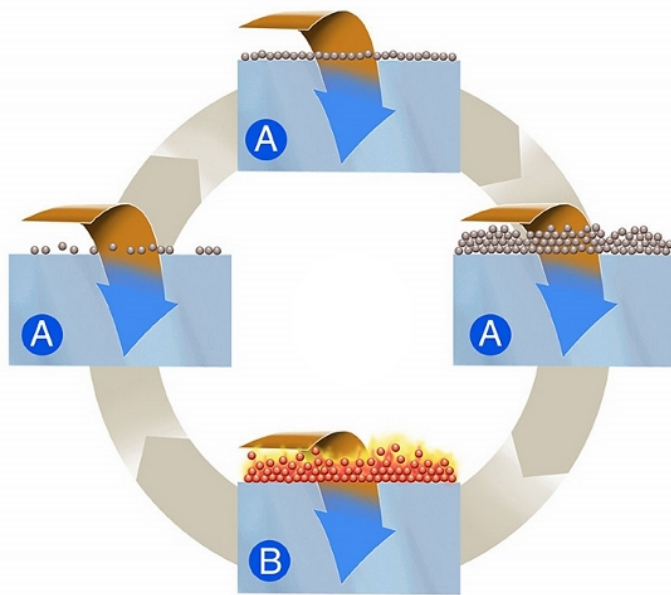


**Figure 5** – Regeneration cycle of particulate filter.<sup>30</sup>

Aside from filtration efficiency and conversion of gaseous pollutants (in the case of catalyzed particulate filter), there are multiple parameters than can be optimized – the priority is to reduce the pressure drop as much as possible for both clean and soot/ash loaded filters.<sup>31</sup> There are key parameters for optimization to reach the best compromise – filter geometry (length, width), microstructure (porosity, pore diameter of both filter substrate and catalytic coating) and channel geometry (channel density, wall thickness, asymmetry).<sup>31, 32</sup>

In the **Figure 6** there are two types of filter geometry – symmetric design and Asymmetric Cell Technology (ACT) Design, developed by Corning Incorporated. ACT design should provide high ash loading capacity with low pressure drop and strength attributes.<sup>31, 33</sup> These filters have larger inlet and smaller outlet channels and therefore a higher volume is available for ash storage in the same space envelope.<sup>9</sup> It can be seen that when the inlet channels contain the same amount of soot/ash, the ACT design channels have thinner soot layer.

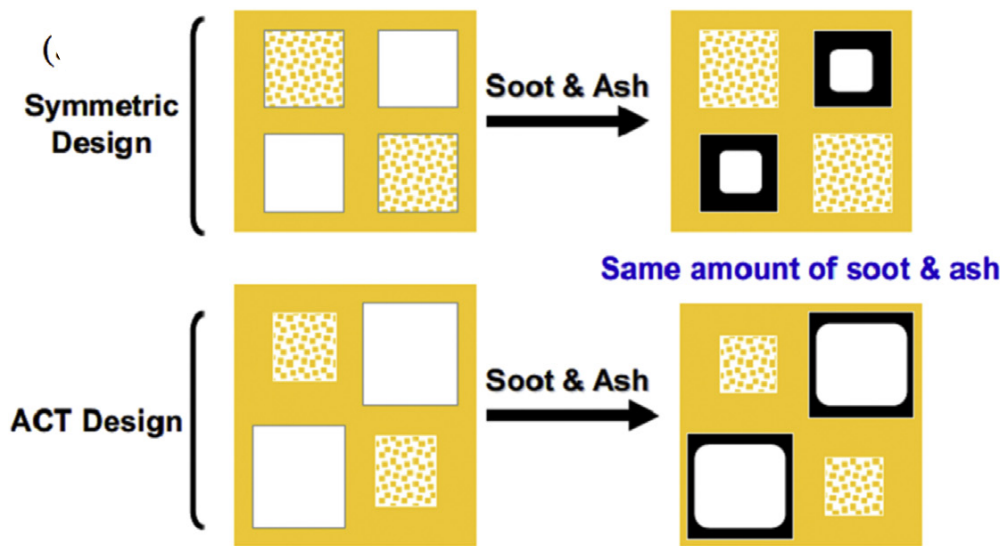


**Figure 6** – Standard and Asymmetric Cell Technology channels comparing with loaded soot.<sup>31</sup>

The Saint-Gobain company developed a new channel geometry, called “wavy”, which is derived from the standard square geometry by adding a sinusoidal undulation of the honeycomb walls as it is shown in the **Figure 7**.<sup>34</sup> They increased the overall inlet channel volume (good for soot/ash storage) and the filtration area (good for backpressure reduction).<sup>9, 33</sup>

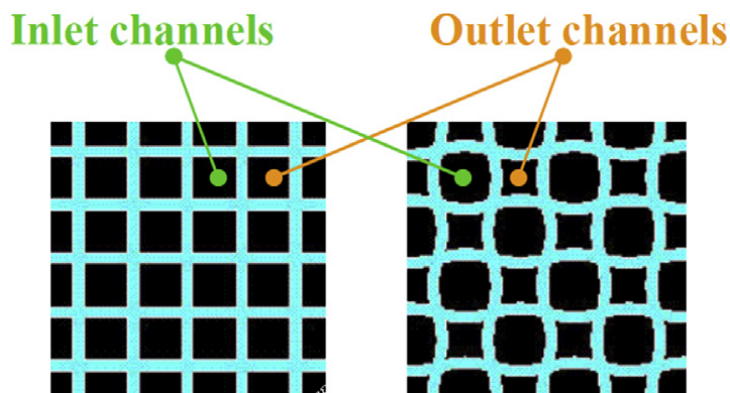


**Figure 7** – Schematic description of standard square cell and “wavy” cell geometry of honeycomb structures.<sup>34</sup>

Particulate filters are placed in exhaust tubing along with various type of flow-through monoliths, which are mentioned above. For Diesel engines aftertreatment there are two options – CSF (Catalysed Soot Filter) or SCRF (Selective Catalytic Reduction Filter).

From the left side the exhaust gases from Diesel engine flow to treatment system as shown in the **Figure 8** and **9**. The catalyst placement of first and second part depends on the arrangement option. Two catalytic parts are connected with pipe where DEF is injected. Then the treatment system continues with SCR. The ASC output flows to tailpipe and now exhaust gases should be harmless.

An example of catalytic converter/filter combination is in the **Figure 8** – DOC with CSF in series (due to heat transfer), followed by a DEF injector (Diesel Exhaust Fluid which is aqueous urea solution), flow-through SCR catalyst and ASC (Ammonia Slip Catalyst), which prevents the release of excess ammonia. CSF contains a layer of oxidation catalyst which enhances the efficiency of soot burn by both O<sub>2</sub> and NO<sub>2</sub>. This is called passive regeneration – it needs higher temperature than 270 °C. The disadvantage of this configuration is that it needs a lot of space due to separate SCR and lower NO<sub>x</sub> conversion is provided specially over cold start, as the SCR takes longer to heat up.<sup>35</sup>

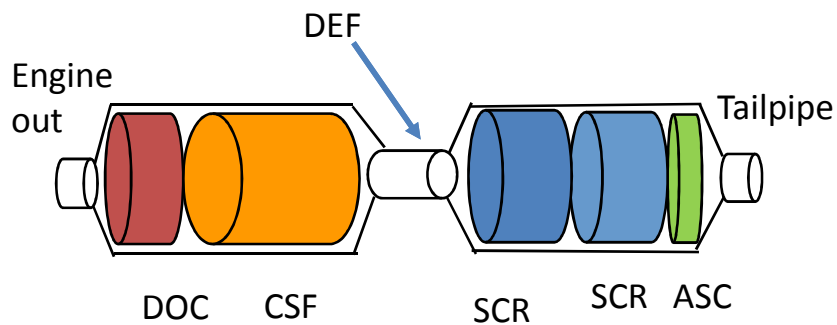


**Figure 8** – Arrangement with CSF of exhaust gas-treatment used for Diesel engines.<sup>35</sup>

Second option does not contain CSF and instead of it, there is SCRF – a filter containing SCR catalyst – as it is shown in the **Figure 9**. The purpose of SCRF is to

reduce NO<sub>x</sub> and also filter soot. Disadvantage is that soot burn efficiency is not as high as at arrangement with CSF, this configuration however takes up less space.<sup>35</sup>

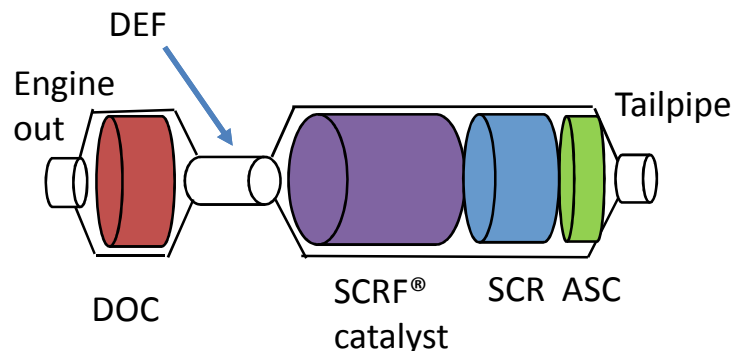


**Figure 9** – Arrangement with SCRF of exhaust gas-treatment used for Diesel engines.<sup>35</sup>

For petrol engines a combination of TWC with GPF (Gasoline Particulate Filter) or cGPF (catalyzed Gasoline Particulate Filter) is used. Gasoline filters operate at higher temperature compared to DPF.

The primary benefit of bare GPF is that it can be designed as stand-alone component which is already optimized with TWC to meet low tailpipe gas emissions. The absence of catalyst allows to achieve high filtration efficiency without any significant pressure drop penalty. In principle, close-coupled TWC could be replaced with a cGPF which is more challenging system due to the higher temperatures and pressure drop.<sup>36</sup> The higher temperature allows an easier regeneration of the filter. It is favorable to combine the catalytic activity for the conversion of gaseous pollutants with the particle reduction in one step. This can be achieved by using cGPF.<sup>37</sup> The overall system is not as complex as for Diesel engines exhaust gases treatment and it can be seen in the **Figure 10** (cGPF can be substituted by bare GPF, except for the third configuration).

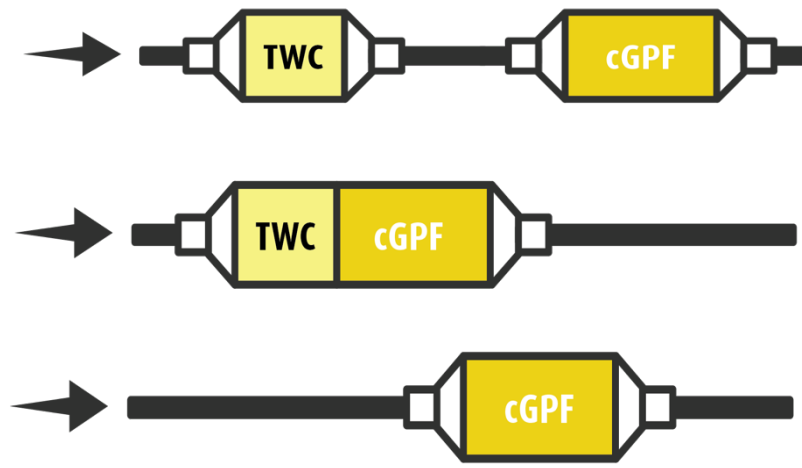


**Figure 10** – TWC with cGPF at various arrangement.<sup>37</sup>

## 2.4 Preparation and Coating of Catalytic Layer

The purpose of this master thesis is to apply thin layers of porous  $\gamma\text{-Al}_2\text{O}_3$  in/onto channels of particulate filters. Nowadays these particles are the widest used support of automotive catalysts. These following factors influence the quality of the layer:

- Coating method;
- Type of used particles;
- Particle size distribution;
- Suspension characteristics;
- Drying;
- Calcination.

Generally there are many coating technics such as<sup>38, 39</sup>:

- Washcoating;
- Wire-wound rod coating;
- Sol-gel method;

- Spin-coating;
- Spray-coating;
- CVD (Chemical Vapor Deposition).

#### 2.4.1 Washcoating

Most of these methods are only suited for coating flat surfaces, however, coating the walls of thing channels inside the monoliths is more challenging. Widely used method in preparation of automotive catalysts is washcoating. The exact procedure of industrial catalytic converter manufacturing (including flow-through converters and monolithic filters) production is a part of know-how. This thesis will focus at dip-coating/vacuum coating methods which mimic the industrial manufacturing.

The principle of dip-coating is to insert sample with defined velocity into solution for specific time. When the sample is in the solution, the sample wets and enters the sample's walls. Due to this effect, particles are trapped on walls as well. Then sample is taken out with defined velocity. Residuum of the solution flows back to the container and the solvent evaporates, as it is shown in the **Figure 11**. Excess of suspension is removed by flowing nitrogen from the side which was dipped in suspension. Other option is to apply the suspension on top of the sample and then pulling it in by connecting the opposite side to the source of vacuum. The last step is drying and calcinating the sample to strengthen the connection of the layer with the support.

The advantages of this method are low-costs, short duration of experiments and variability. The properties of applied layer is influenced by many factors, however, when the procedure is controlled, catalytic layers with desired well-defined characteristics can be prepared.

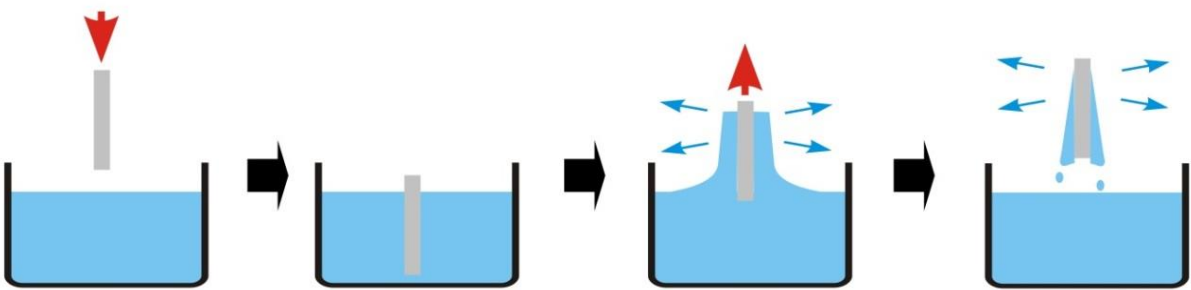


**Figure 11** – Dip-coating method.<sup>14</sup>

#### 2.4.2 Properties of $\gamma\text{-Al}_2\text{O}_3$ Particles

Aluminum oxide has several various crystalline modifications but the  $\gamma\text{-Al}_2\text{O}_3$  crystalline modification is widely used as catalyst support. It is easy to prepare, forms highly porous particles with different meso-porous size and they are thermally stable. Due to high porosity with thin pore size distribution they have a large specific surface area (from 90 – 210 m<sup>2</sup>/g<sup>40</sup>), where nanoparticles of active metals can be dispersed. They are obtained by dehydration from monohydrate Al<sub>2</sub>O<sub>3</sub> (boehmite) at temperature 400 – 450 °C and to improve their structural properties, precipitation or hydration is used.<sup>41, 42</sup>

The most significant property of  $\gamma\text{-Al}_2\text{O}_3$  particles for suspension preparation is their amphoteric character. It means that they interact with both negative and positive ions in aqueous media – between aqueous ions and  $\gamma\text{-Al}_2\text{O}_3$  particles dielectric bilayer is created. This charge can be modified by changing pH. The overall charge can approach zero and this point is known as isoelectric, at which the suspension is turned into gel-like state (the particle concentration needs to be high enough). The highest achieved viscosity at the isoelectric point indicates that van Der Waals's forces play a significant role. In this state the suspension behaves as pseudoplastic fluid<sup>43, 44</sup>, which is the most interesting state for dip-coating on monolith wall and monolithic filter walls.

### 3 EXPERIMENTAL PART

All steps of sample preparation is illustrated by **Figure 12**. On the left side all main components are written and there are connected with the boxes by blue arrows. The boxes represent procedure. On the right side the key parameters are pointed and marked with orange darts.

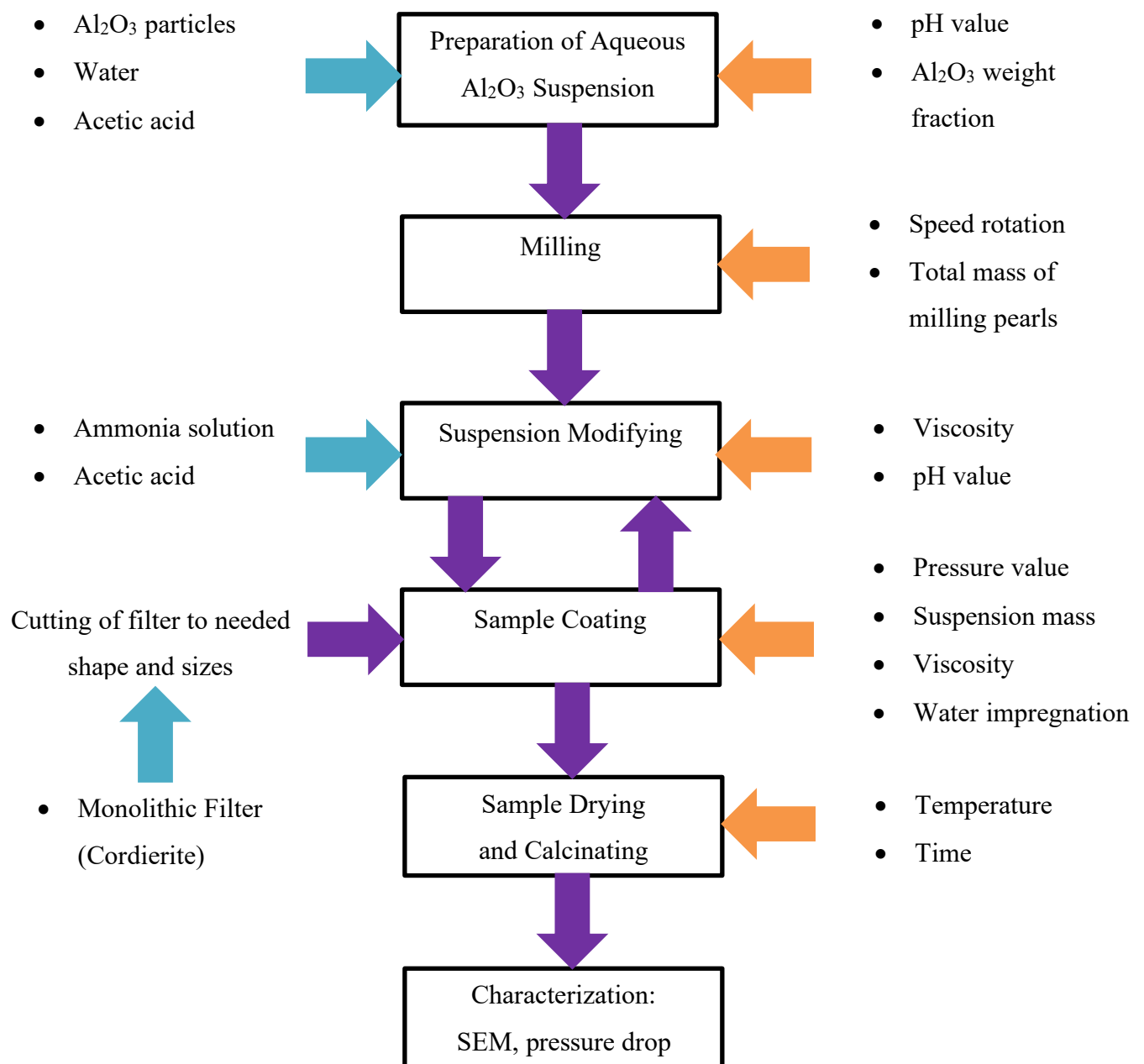


**Figure 12** – The sketch of sample preparation with all steps, important parameters and components.

### 3.1 Preparation and Characterization of Aqueous Suspension

In this master thesis  $\gamma$ -Al<sub>2</sub>O<sub>3</sub> particles were used because they are the most often used as a catalytic support in automotive catalysts. These particles are manufactured by Sasol company and their product is called SCFa140. Company declares their specific area around 140 m<sup>2</sup>/g with thin mesoporous distribution about 10 nm.<sup>40</sup> All characteristics of SCFa140 are described in **Table 3**.

**Table 3** – SCFa140 all characteristics.<sup>40</sup>

<b>Al<sub>2</sub>O<sub>3</sub></b> [wt. %]	95	<b>Loose bulk density</b> [g/dm <sup>3</sup> ]	500-700
<b>Na<sub>2</sub>O</b> [wt. %]	0.002	<b>Packed bulk density</b> [g/dm <sup>3</sup> ]	700-1000
<b>La<sub>2</sub>O<sub>3</sub></b> [wt. %]	3	<b>Range of surface area BET</b> [m <sup>2</sup> /g]	140
<b>L. O. I.<sup>1</sup></b> [wt. %]	2	<b>Pore volume</b> [ml/g]	0.5
<b>Particle size d<sub>50</sub></b> [μm]	35.5	<b>Pore radius</b> [nm]	8

The suspension preparation was always the same but the milling time was dependent on desired particle size. Firstly, particles are mixed with distilled water to obtain suspension with 38 wt. % of particles. The next step is to modify the pH to 4.5 with adding acetic acid. The suspension is then put into the pearl mill with recycle – Eiger Torrance LTD M100.

---

<sup>1</sup> L. O. I. = loss on ignition

If the suspension parameters and the mill set-up (shown in the **Table 4**) are the same, the milling kinetic is reproducible as the **Figure 13** – Dependence of volume particles size on milling time determined by  $d_{90}$ ,  $d_{50}$  and  $d_{10}$ . illustrates. The changes of particle size are described by  $d_{10}$ ,  $d_{50}$  and  $d_{90}$  – e. g.  $d_{90}$  (90 % quantile) indicates that 90 % of volume of particles have the size/diameter “ $d$ ”.

**Table 4** – Description of mill set up and suspension parameters.

Suspension parameters		Mill set up	
<b>pH [-]</b>	4.5	<b>Speed rotation [rotation/min]</b>	3500
<b>Suspension volume [ml]</b>	400	<b>Total mass of milling pearls [g]</b>	259.6
<b>Weight fraction of particles [%]</b>	38		
<b>Particles size before milling <math>d_{50}</math> [<math>\mu\text{m}</math>]</b>	35		

After milling, volume particle size distribution (PSD) is measured by laser diffraction granulometry (HORIBA Partica LA-950V2). The principle is based on static light scattering – larger particles diffract light with larger angles but with lower intensity. When diffraction indexes and absorption coefficients of solid material and solvent are known, the PSD can be calculated more precisely with using more detailed algorithm.<sup>45</sup>

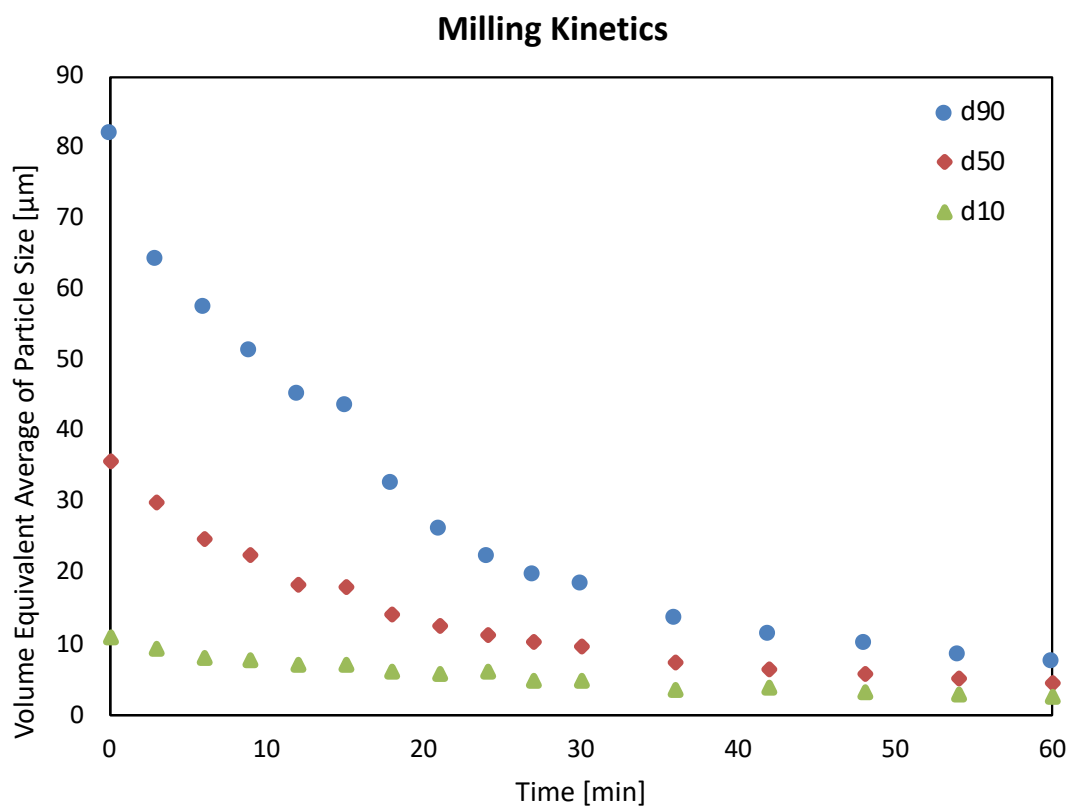


**Figure 13** – Dependence of volume particles size on milling time determined by  $d_{90}$ ,  $d_{50}$  and  $d_{10}$ .

After milling on desired particles size, the pH is changed again to be close to the isoelectric point. In this point the suspension behaves as pseudoplastic fluid and it has the highest viscosity. The modifying is provided by adding ammonia aqueous solution in small doses while the mixture is stirred continuously. In case of many suspensions, the “gelation” (changeover to gel-like state) is around at pH 7. The rheologic behavior of suspensions was measured at rotational viscometer- Anton Paar Rheolab QC.

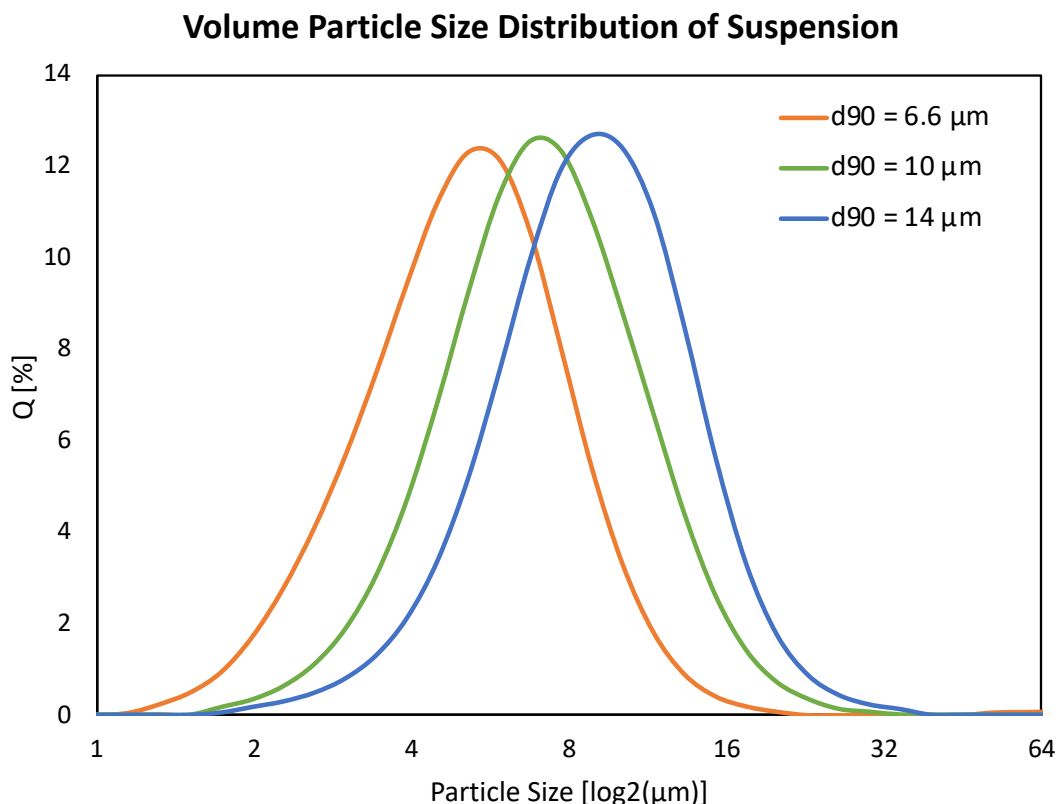


**Figure 14** – Volume particle size distribution of all used suspensions.

To investigate the influence of PSD on the catalyst distribution in monolithic filters and to optimize dip-coating and vacuum methods on the filters, four suspensions with different PSD and pH (connected with viscosity) were prepared, the parameters are summarized in the **Table 5**. Volume PSD ( $d_{90}$  of particles) of all prepared suspensions are illustrated in **Figure 14** – Volume particle size distribution of all used suspensions. The reason for  $d_{90}$  is that the gelation procedure is sensitive to the presence of very large particles – only a small number of them can prevent the turnover to gel-like state.  $d_{90}$  is an useful indicator that they are not present in the suspension.

**Table 5** – The overview of all parameters of used suspensions.

$d_{90}$ [ $\mu\text{m}$ ]	pH [-]
<b>6.6</b>	7.05
<b>6.6</b>	6.6
<b>10</b>	6.6
<b>14</b>	7.3
<b>14</b>	6.8
<b>14</b>	6.6

### 3.2 Coating of Monolithic Filter

The sample preparation composes of several steps which had to be handled (they are described in detail in chapters below):

- Cutting of filter – cuboidal- and cylindric-shaped samples;
- Removal of excess suspension – flow distributor and vacuum coating;
- Drying;
- Calcination.

In this master thesis, two types of samples were used – cuboidal- and cylindric-shaped. The purpose of cuboidal samples was to try how the coating of filters behaves and to find out parameters suitable for coating of cylindric samples. All samples were made from the same material provided by NGK Ceramics company – porous cordierite. The first tests consisted of dip-coating cuboidal samples because this method was already applied on flow-through monoliths in our research group and crucial parameters are known<sup>10</sup>.

### 3.2.1 Cuboidal Samples

Cuboidal samples had sizes and shape as they are sketched in the **Figure 15**. They were coated in similar way as flow-through samples which consists of two main steps. Generally, the first step is to get the prepared suspension (aqueous solution of  $\gamma\text{-Al}_2\text{O}_3$ ) into sample and then to remove it, leaving just a thin uniform layer on walls of channels.

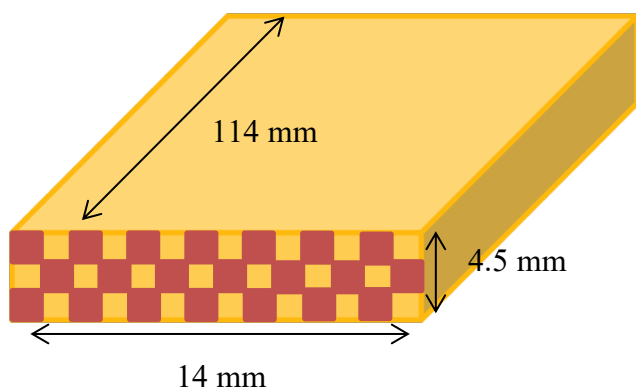


**Figure 15** – The sketch of cuboidal samples with sizes.

In this work the dip-coating method was slightly modified. Due to length of the sample it was not possible to use the apparatus which was built for coating of flow-through samples (they were much shorter). The filters were therefore dipped in the suspension manually.

Firstly, sample was weighted using analytical scales and suspension was put into thin vessel. Before the coating, exterior of the sample had to be covered in PTFE tape to ensure the suspension is not on outer sample area and also to seal the sample in the holder during blowing through. The speed of dipping/pulling out and immersion were kept the same for all samples, see **Table 6**, with minor variations due to manual coating. In the right side of the **Figure 16**, the directions of dipping and blowing out are shown.

**Table 6** – Overview of dip-coating steps of cuboidal samples.

Movement	Time [s]
Dipping	15
Dipped	60
Taking out	15

When the sample was pulled out, the excess of suspension needed to be removed. For this operation, a device illustrated in the left side of **Figure 16**. This device is connected to a pressurized nitrogen bottle with a regulation valve. The sample was inserted in the device by the side that was dipped into suspension to increase the coating depth (to “push” suspension deeper). The pressure set on the reduction valve is a significant parameter influencing the coating length, layer thickness and uniformity and will be mentioned for each sample.

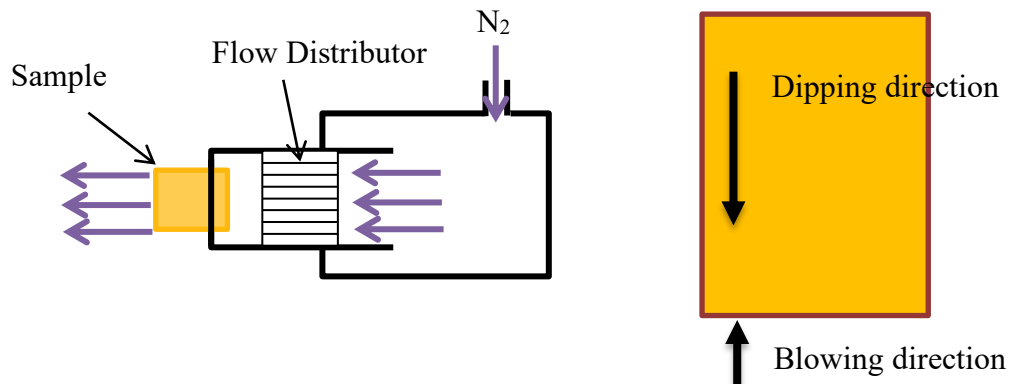


**Figure 16** – Scheme of blown device and direction paths.

The samples were then dried in a drying cabinet set up at 40 °C for approx. 1.5 hours – weight of the sample was observed (dry sample absorbs humidity and its weight is increasing again). Dried sample was weighed without the PTFE tape and calcined in furnace. The temperature was increased by 10 °C/min until 500 °C, at which it was

kept for 120 min. The samples were then cooled passively because the furnace does not have active cooling system.

### 3.2.2 Cylindrical Samples

The principle of all steps described above are similar to preparation procedures with cylindric samples and therefore it is not deeply described. Cylindrical samples were cut by metal saw and ground off by inserting in a tube of desired diameter. The sample is sketched including dimensions in **Figure 17**. The grounding tube had the same size as the tube which is part of apparatus – see **Figure 18**. The samples were then weighed and covered by PTFE tape. Then it was slowly inserted into the plastic tube of apparatus, so the sample is not damaged by sample-holders.

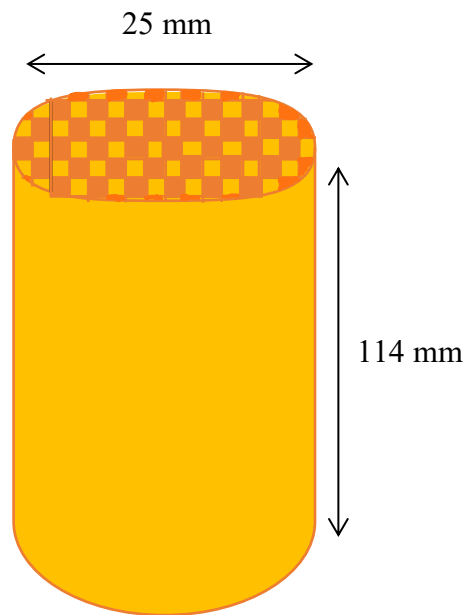


**Figure 17** – The sketch of cylindrical samples with sizes.

The sample holder needed to be connected to vacuum source. The schemes of the sample holder tube and the funnel are shown in the **Figure 18** and **18** including dimensions in *mm*. They were 3D printed from PLA (polylactic acid) – the used printer was PURUSA i3 MK3S with 80 % of wall-filling. The tube with 6 sample-holders

where sample sits on is shown in the **Figure 18**. On the left side the solid line is center-line of the object. Internal diameter is a little larger to fit the sample accuracy. Wall-filling and the wall size was chosen to resist of damage caused by vacuum. It is longer than the sample in order to have additional space where the suspension is loaded. The bottom part fits in the funnel. Length from bottom to the sample-holders was designed not to influence air flow through filter in the case the tube does not fit tightly in the funnel – sometimes there can be a small gap.

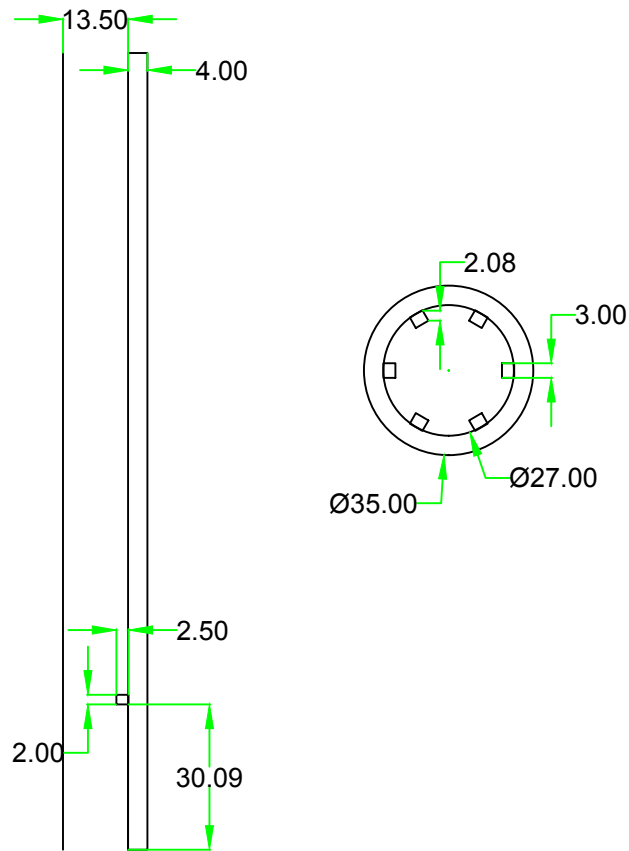


**Figure 18** – The lay-out of the tube from cut- and vertical projection with all sizes.

The **Figure 19** shows the drawing of the funnel (two parts on the left side) and the whole printed and assembled sample holder connected to vacuum hose (photo on the right), which is mounted to the funnel and secured by a clamp. The hose is connected to

a 50 litre tank equipped with a liquid separator and, finally, an oil vacuum pump – Becker U 4.20. There is a valve on the air tank (marked as B – see **Figure 19**) which can be opened to atmosphere and can be used to control the pressure inside the tank. The pressure is an important parameter for vacuum coating to obtain uniform layer and coating length.

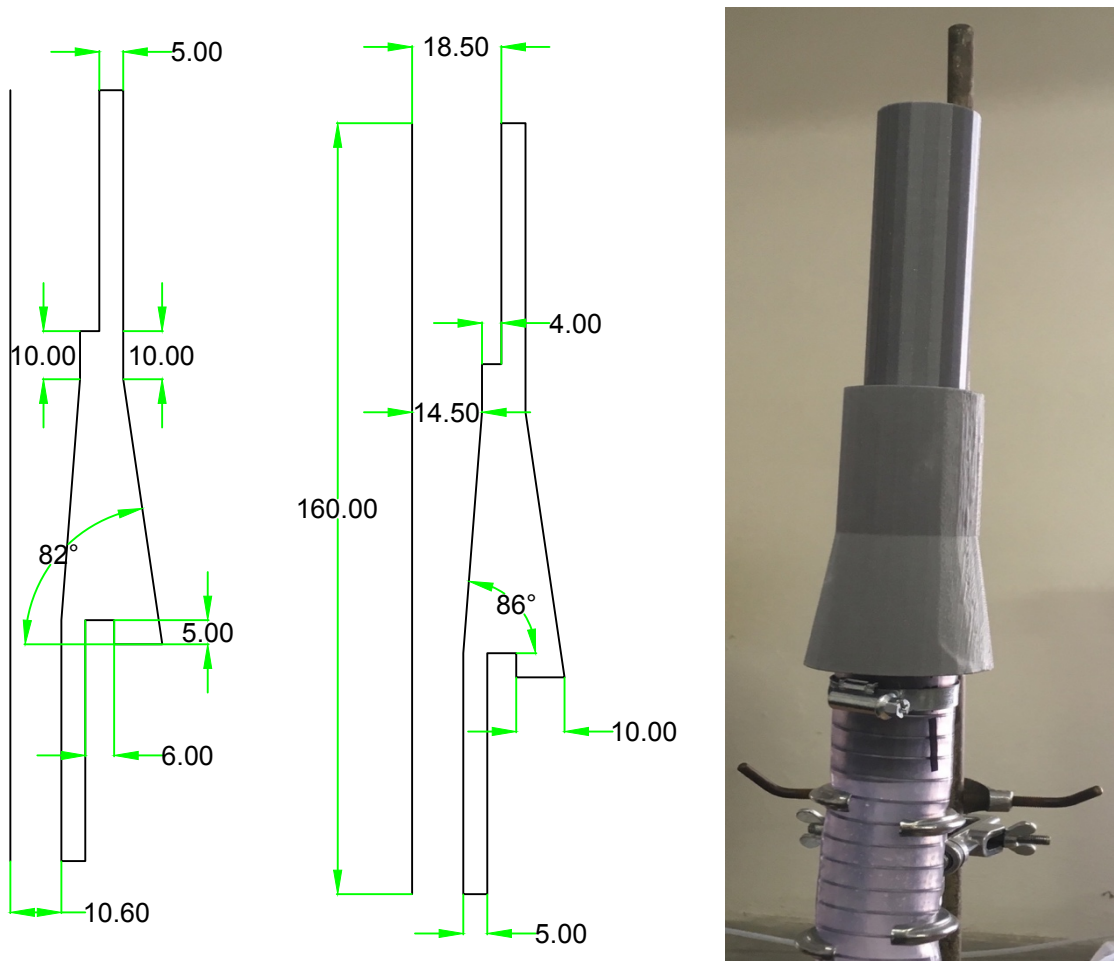


**Figure 19** – The lay-out of the funnel from cut-projection with all sizes and printed and assembled apparatus with vacuum system.

The vacuum value was set up by valve B (see **Figure 20**) on the air tank when sample with tube was arranged together with funnel. There were three values used: -1, -0.8 and -0.6 barg. After opening the valve A between the sample holder and the tank,

pressure difference could damage the sample – in worst scenario it can be “sucked” in. Therefore, for the first experiment, the valve A was fully opened and the pump was kept on, but the coating length was too short. For further experiments, the pump was only used to evacuate the tank to desired pressure and afterwards the valve A was opened. The steps following the coating were the same as for cuboidal-shaped samples.

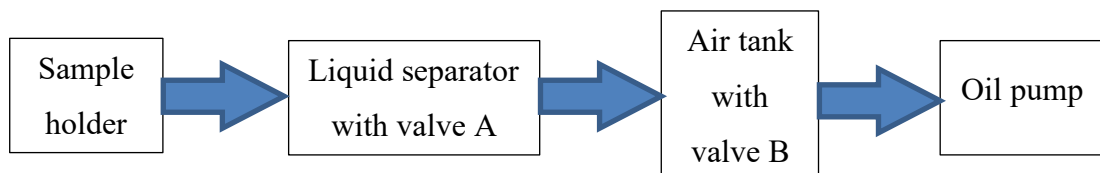


**Figure 20** – Scheme of vacuum coating apparatus.

### 3.3 Pressure Loss of Filters

Pressure loss is one of the most important parameters of particulate filters as described in **Literature Review**. In this thesis pressure loss of both coated and bare cylindric filter samples were measured. The measurements were done with nitrogen at room temperature. The nitrogen vessel was connected to 500 dm<sup>3</sup>/l MFC (Mass Flow Controller) by company Bronckhorst. The desired flow rate can be set on the control unit connected to the MFC. Pressure detectors are placed in front of and behind the sample and they are connected to pressure measuring device. The range of sensor is 10 kPa. In the **Figure 21** the sketch of whole procedure is illustrated.

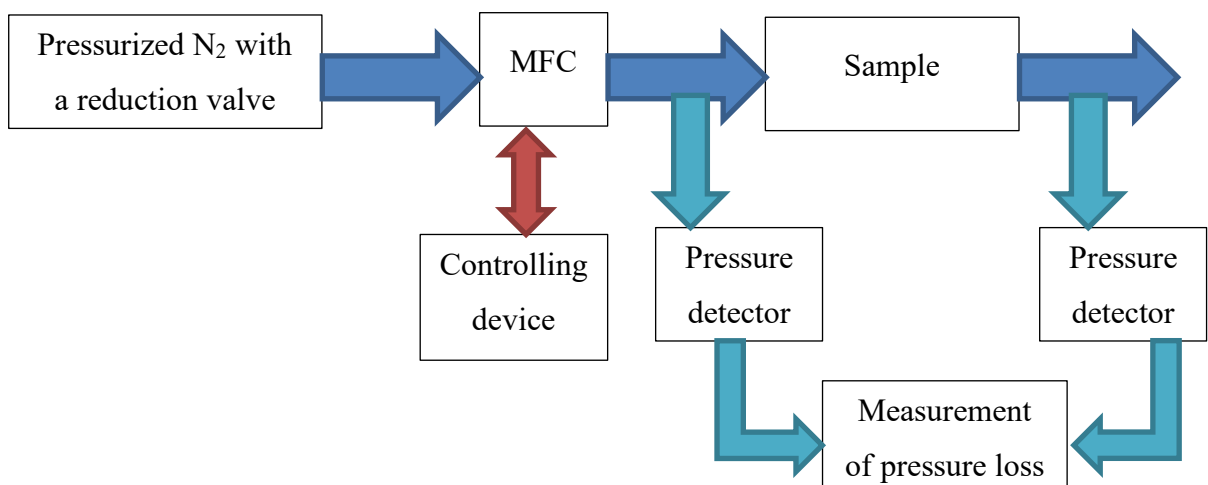


**Figure 21** – Sketch of pressure loss measurement.

**Figure 22** shows the sample and pressure detector connections. The sample was wrapped by PTFE tape and inserted in two tubes. This whole arrangement was covered by shrink-tube which was warmed up by heat gun – the shrink-tube lowered its diameter, wrapped the sample tightly and sealed it. Strapping tapes tighten the tubes and shrink foil together.

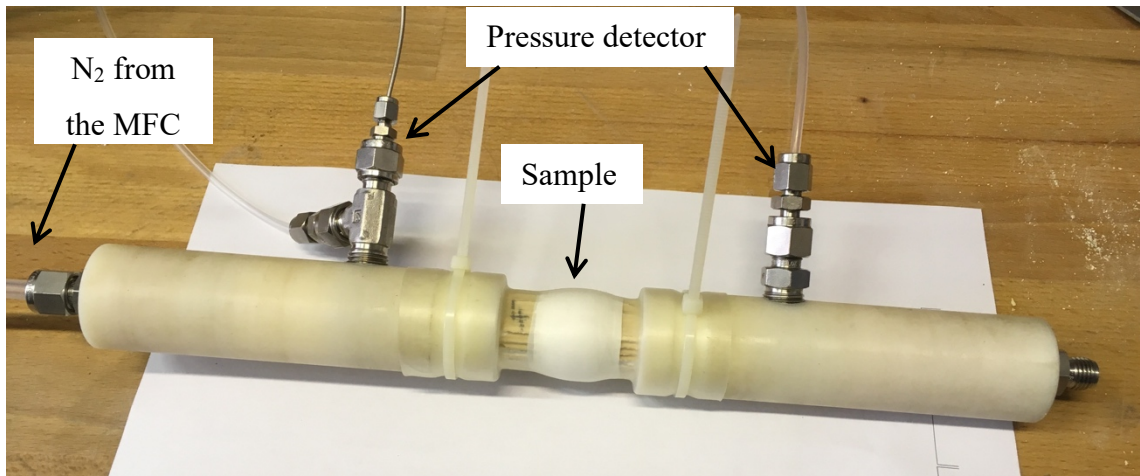


**Figure 22** – Photo of sealed sample prior to the pressure drop measurement.

### 3.4 Analysis of Coated Samples

After coating procedure and measuring pressure loss, it was needed to analyze coated length and layer thickness on the walls of channels. Sample had to be cut across by metal saw into 1 cm long pieces, starting from the dipped side, to investigate coated length. Layers formed by  $d_{90} = 14 \mu\text{m}$  particles could clearly be seen by human eye (**Figure 23**), in the case of  $6.6 \mu\text{m}$  particles, only a thin white cover could be seen on the substrate under strong light.

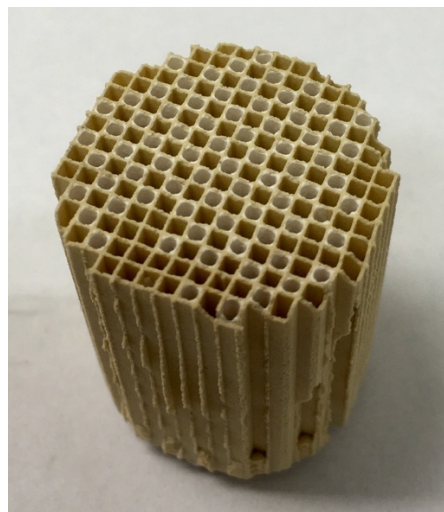


**Figure 23** – Cut cylindric sample to investigate coated length (sample coated by  $d_{90} = 14 \mu\text{m}$  suspension). Almost all inlet channels are coated – the layer is clearly visible.

The coated layers were characterized by SEM (Scanning Electron Microscope) – Tescan Vega 3SBU. It is equipped with SE (Secondary Electrons), BSE (Backscattered Electrons) and TE (Transmission Electrons) detectors. In this work, only the BSE detector was used because it offers higher contrast between different phases, in comparison with SE. Thermo-emissive wolfram cathode was the source of electrons and accelerating potential was set up to 20 kV<sup>45</sup>.

Samples were cut on slices in every centimeter and it was chosen 5 cm slice for comparing. This method can lead to experimental errors – e.g. the layer thickness was not statistically observed. A selected slice of the coated filter was placed into plastic vessel and filled by epoxy resin. The resin provided sample fixation. When it solidified, the sample was ground using SiC sandpaper and polished by colloid silica at lapping and polishing machine South Bay Technology 910. The polished sample was then washed, dried and metal-coated with a 20 nm thick layer of gold, which conducts electrons away during scanning by SEM and prevents charging of the sample.

Scanned photos were analyzed by ImageJ software for image analysis to evaluate coated layer thickness and the ratio between in-/on-wall particles.

## 4 RESULTS AND DISCUSSION

In this work, many samples were coated with various parameters, which are influencing the coating procedure and layer thickness, such as PSD, pH (connected with viscosity), vacuum coating pressure, the effect of wetting the substrate with water prior to the coating (further referred as “wet samples”) and additional sealing of the apparatus. The purpose was to find, compare and select significant phenomena which influence the whole coating process. This chapter is mainly focused on vacuum-coated cylindrical samples because further research will aim to adding active metals to Al<sub>2</sub>O<sub>3</sub> layer and then catalyst activity will be studied in a tubular reactor.

### 4.1 Dip-coating of Cuboidal Samples

The purpose of dip-coating experiments with cuboidal samples was to find out and verify suitable parameters for vacuum coating of cylindrical samples. The  $d_{90} = 14 \mu\text{m}$  suspension was used with various pH modified by acetic acid – 7.3, 6.8 and 6.6 – all suspensions were in gel-like state. The pH directly influences viscosity – suspension with pH 7.3 had the highest viscosity and with decreasing pH the viscosity also decreases (for pH 6.6 viscosity is the lowest), see **Figure 24** (a dependency of apparent viscosity on shear rate). Additional viscosity measurements are enclosed in **Appendix**.

Samples were dipped into suspension with various pH and then the excess was removed by pressurized nitrogen – the pressure set by the reducing valve was 4 bar. The influence of nitrogen pressure was studied previously and 4 bar was chosen as the best operating pressure.<sup>10, 14</sup>

The coated lengths (the distance along the sample channels, at which a coated layer is still apparent) while using suspension with various pH are compared in **Figure 25** and it is seen that the pH is significant parameter for the length. Dip-coating was tried also with lower pH but it was not optimal – the suspension penetrated around the sample even when they were wrapped by PTFE tape.

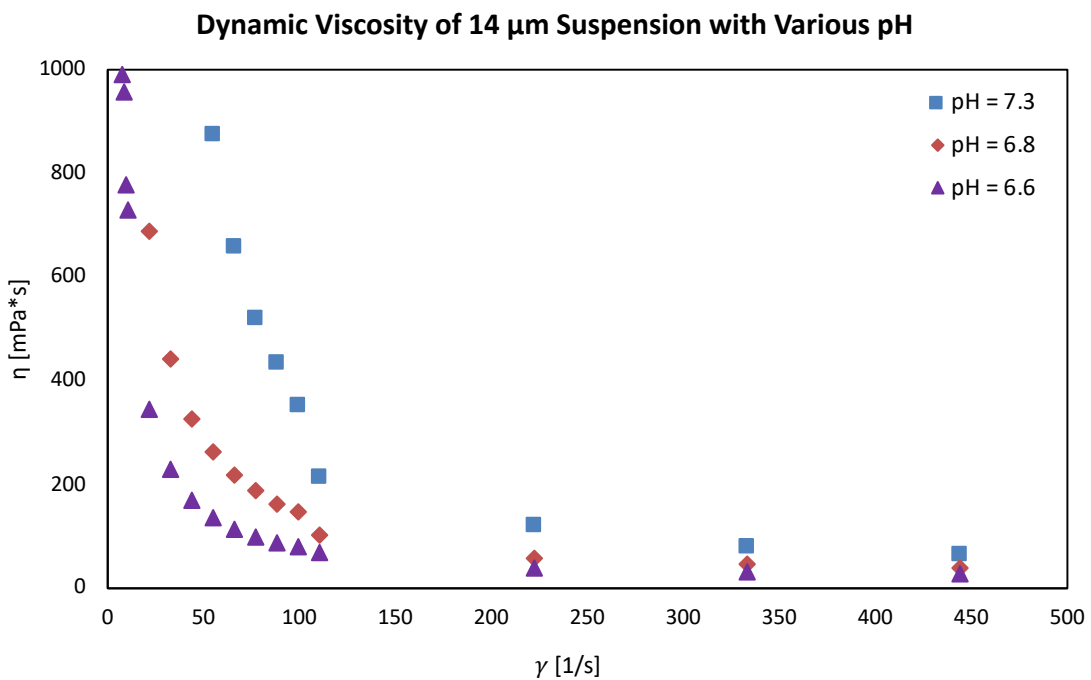


**Figure 24** – Comparing dynamic viscosity of suspensions with  $\text{pH} = 7.3$ ,  $6.8$  and  $6.6$  for the  $d_{90} = 14 \mu\text{m}$  suspension.

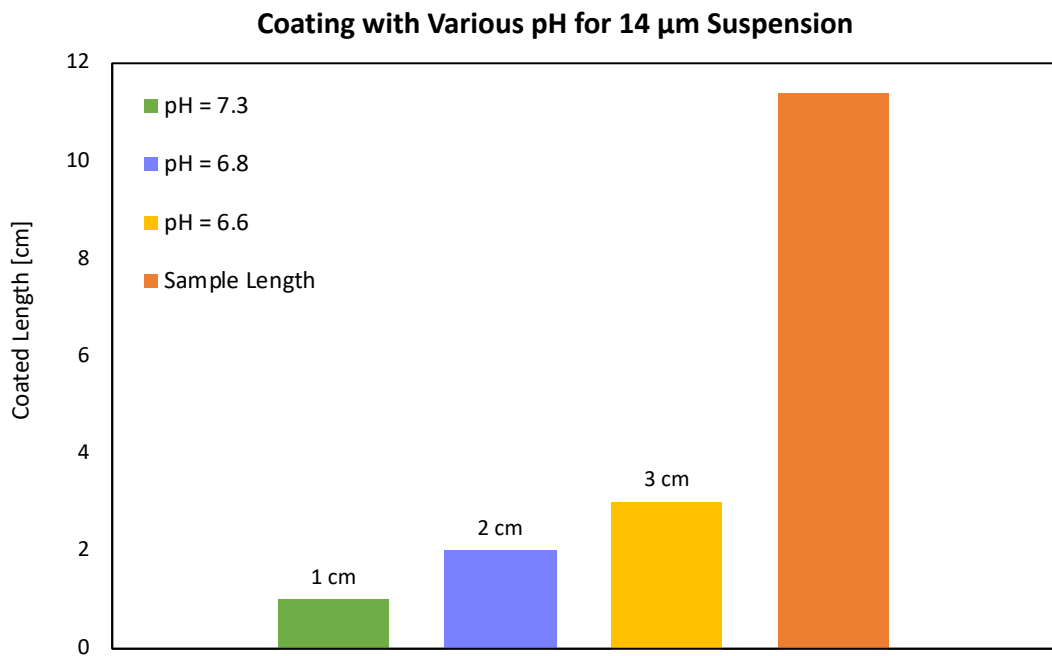


**Figure 25** – Comparing coated length of  $d_{90} = 14 \mu\text{m}$  suspension with various pH for dip-coated cuboidal samples.

**Figure 26** shows a single channel from sample dip-coated with  $d_{90} = 14 \mu\text{m}$  suspension with pH = 6.6. It can be seen that a thick and compact layer (gray color) was formed while a small amount of the suspension penetrated into the walls.

For further work, pH = 6.6 was chosen as a suitable parameter but this trend (with lower pH, the coating length is increasing) was always verified.

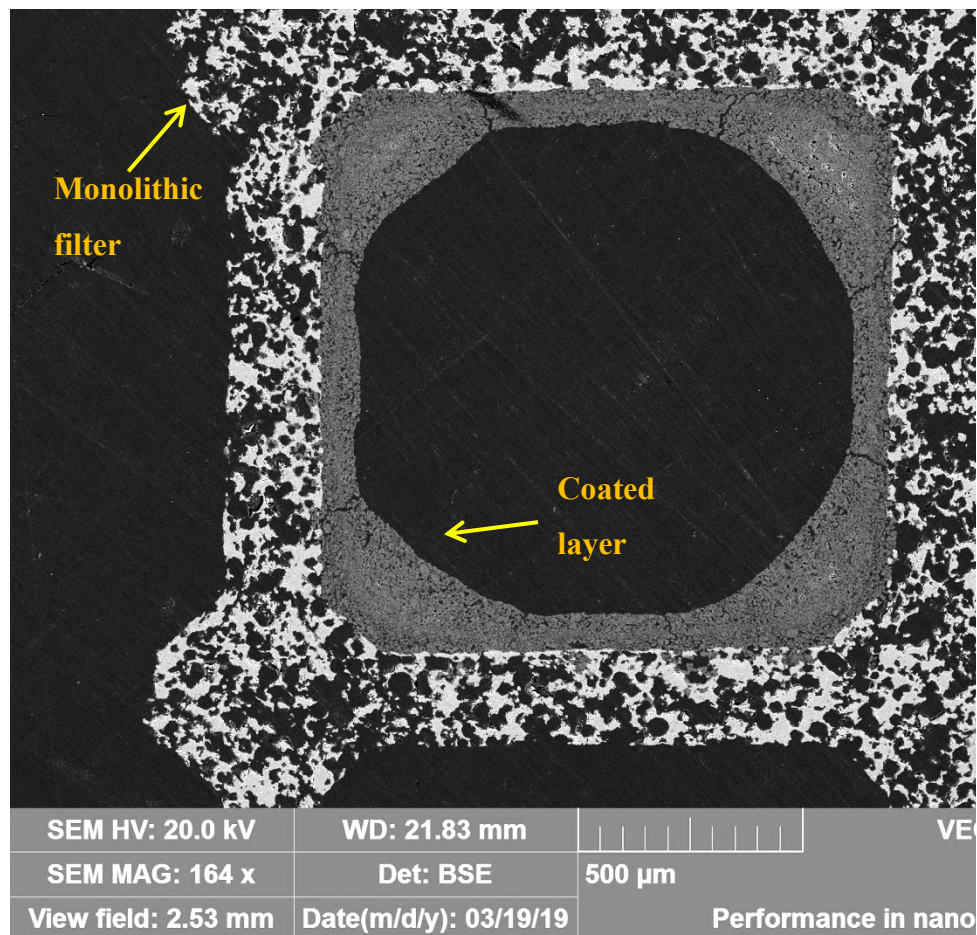


**Figure 26** – SEM micrograph of a single channel from a sample dip-coated with a  $d_{90} = 14 \mu\text{m}$  suspension with pH = 6.6.

## 4.2 Vacuum Coating of Cylindrical Samples

In this chapter all crucial parameters which influence coating length, layer thickness and uniformity are investigated similarly as for the dip-coated samples but this time for the vacuum coating procedure.

### 4.2.1 Suspension Loading

First of all, it is important to know how suspension loading affects the coated length. Samples were coated by three various amounts of suspension with pressure set at  $-0.6$  barg, particle size  $d_{90} = 10 \mu\text{m}$  and pH = 6.6. Compared results are illustrated in **Figure 27** – for loading 3 g the length is 3 cm, for 6 g the distance is 5.5 cm and for 10 g the length is 8.5 cm. Sometimes, few channels were not coated in the same length as the rest. The aim was to coat at least half of the sample length – approx. 6 cm – so when the samples are coated from both sides, there is no uncoated region in the middle of the sample. In further experimental work, 6 g of suspension was mostly used. When the samples were coated from both sides and were intended for pressure loss measurement, 10 g of suspension was used to avoid uncoated regions. Graph of dynamic viscosity is enclosed in the **Appendix – Figure 41**.

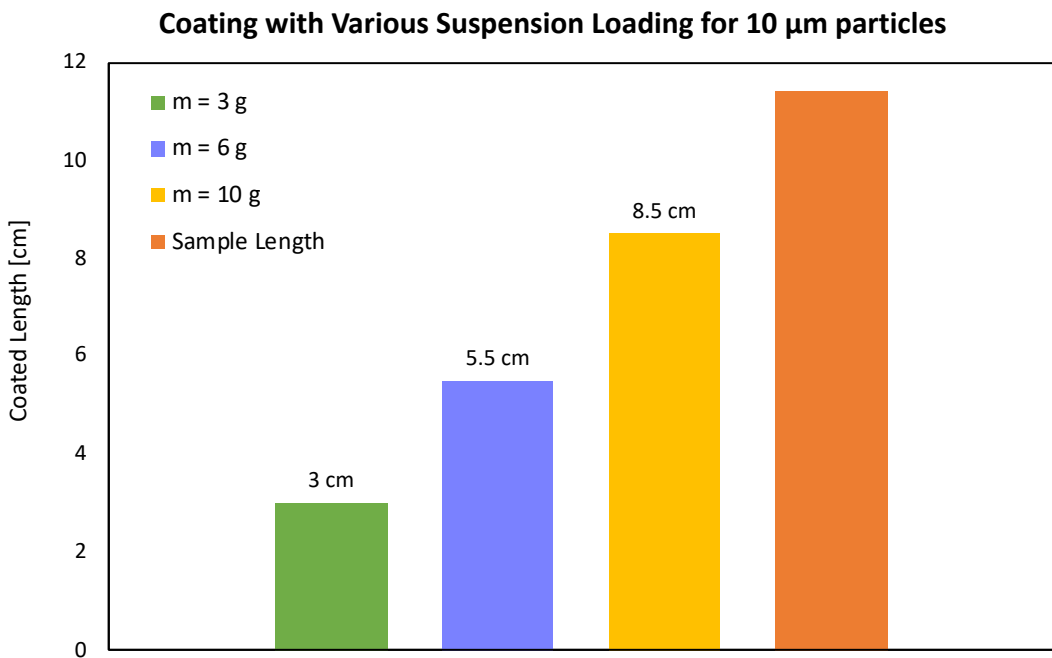


**Figure 27** – Dependency of coated length on suspension loading on for  $d_{90} = 10 \mu\text{m}$ .

#### 4.2.2 Suspension pH

pH is the crucial value for coating because it is directly connected with viscosity. The highest viscosity is obtained when pH is modified as close as possible to the isoelectric point. For the dip-coating experiments, the highest coating distance was reached for pH = 6.6.

Based on this knowledge, cylindrical samples were vacuum-coated by suspension with pH = 7.3, 6.6 and 6.1. The pH value 7.3 was the closest to isoelectric point, at 6.1 the viscosity was very low even when no external force was applied, closer to liquid than to gel. The pH = 6.6 suspension was in gel-like state (when no external force applied), which has some advantages – suspension did not penetrate into the sample before the vacuum was applied, and no regions with local higher density of solid phase by water penetration to the porous substrate were present. The pH = 6.1 suspension behaved as a liquid and it was not possible to load more than 2 g of the suspension on the sample

because it immediately penetrated into the sample and the gaps between PTFE tape and sample, and PTFE tape and the tube.

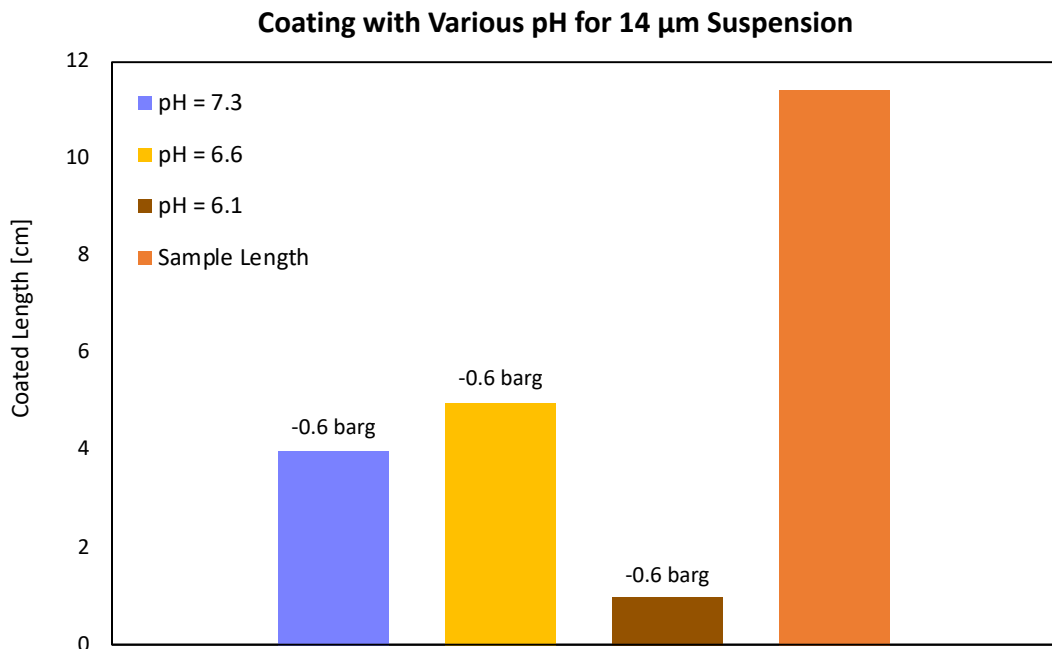


**Figure 28** – Suspension  $d_{90} = 14 \mu\text{m}$  coating with various pH.

The results of several experiments can be seen in **Figure 28** and **Figure 29**. 6 g of suspension and the same pressure ( $-0.6 \text{ barg}$ ) were used, but the  $d_{90}$  varied (14 and  $6.6 \mu\text{m}$ ), respectively.

The coated length was 4 cm for both suspensions in isoelectric point (pH = 7.3 for  $14 \mu\text{m}$  and  $7.05$  for  $6.6 \mu\text{m}$  particles) and for the same pH value (6.6) the length was also the same – approx. 5 cm. When the pH was 6.1 the sample was not coated well, because the suspension penetrated into the sample immediately without using vacuum and channels were plugged by local solid phase (water penetrates faster into the substrate which leads to local increase of solid fraction).

These values are slightly different by previous study (various suspension loading), but it is caused by experimental errors – sealing could be different (tube-sample and

tube-funnel), length was surveyed by human eye and suspension with particle size  $6.6 \mu\text{m}$  is seen very poor even under strong light and experiments were not statistically analyzed. The coated length of 5 cm is still a good result because the aim was to have coated distance up to the half of sample length which could be obtained by increasing suspension loading. In both **Figures** results are illustrated.

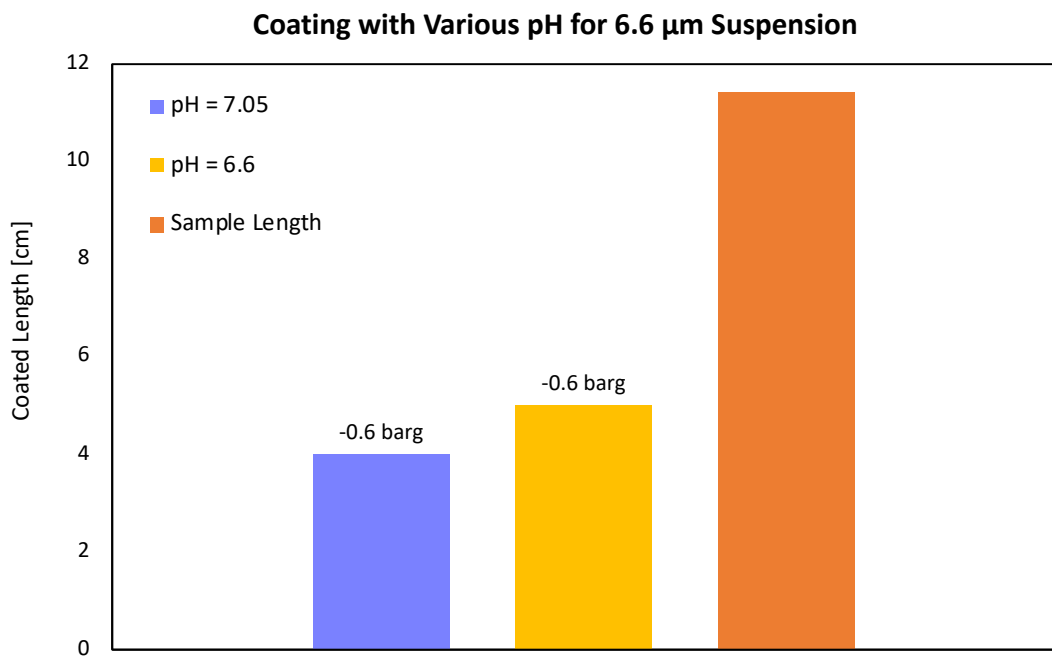


**Figure 29** – Suspension  $d_{90} = 6.6 \mu\text{m}$  coating with various pH.

Overview of apparent viscosity is shown in **Figure 41** enclosed in **Appendix** for both suspensions with their pH. The values for particles size  $6.6 \mu\text{m}$  with pH 7.05 are not shown – the measurement was not successful even though it was repeated many times because the viscosity was too high and the space between the two cylinders in the viscosimeter could not be properly filled.

#### 4.2.3 Pressure During Vacuum Coating

Vacuum is one of the parameters which were studied. Two pressure values were chosen:  $-0.6$  and  $-0.8$  barg. Lower pressure was not investigated so the samples were not damaged. This study was aimed at two different suspensions ( $d_{90} = 14$  and  $6.6 \mu\text{m}$ ) with the same pH 6.6 and with 6 g loading, see **Figure 30** and **Figure 31**. Both suspensions reached the same coated length 5 cm when vacuum was  $-0.6$  barg. Different results were obtained when the pressure was set to  $-0.8$  barg – coated length for  $14 \mu\text{m}$  particles was 5.6 cm and for  $6.6 \mu\text{m}$  it was 6 cm. The coating length was slightly higher when  $-0.8$  barg was applied, however, the difference was not very high (5.6 vs. 5 cm) and for further experiments, vacuum  $-0.6$  barg was used as a standard coating procedure.



**Figure 30** – Coated length of various pressures set for the vacuum coating of  $d_{90} = 14 \mu\text{m}$  suspension.

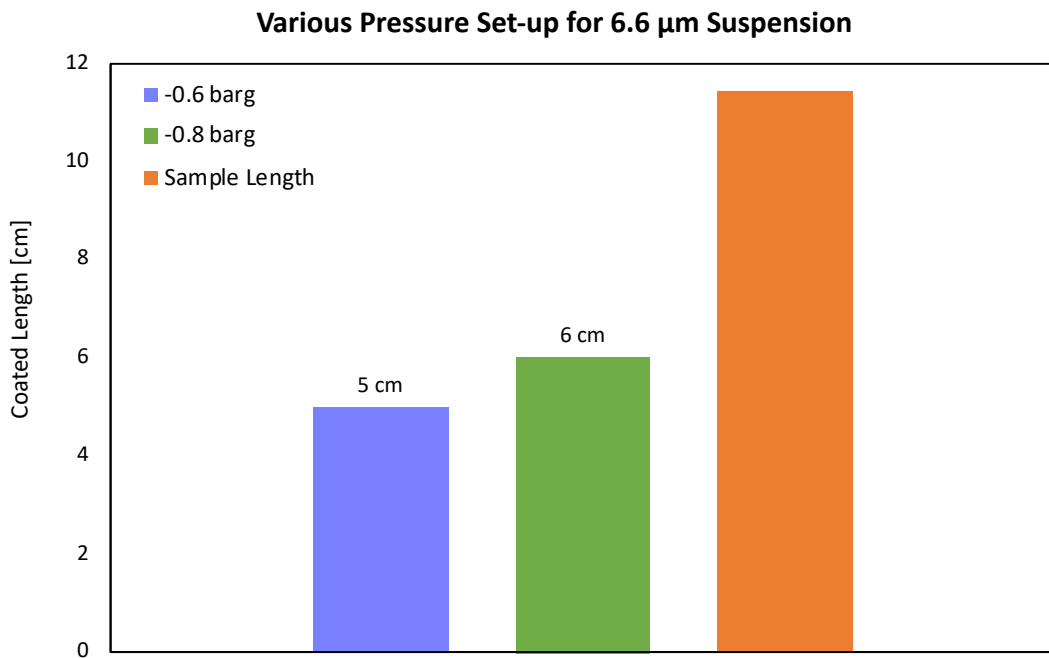


**Figure 31** – Coated length of various pressures set for the vacuum coating of  $d_{90} = 6.6 \mu\text{m}$  suspension.

#### 4.2.4 Particle Size

This subchapter is focused to compare how vacuum and suspension PSD influence the layer thickness in coated channels. When samples were coated they were imaged by SEM and layer thickness were measured in ImageJ software. Layer thickness in every coated corner was measured under  $45^\circ$  angle and all samples have the same distance from the suspension loading side, corresponding to the coating length = 5 cm.

The results are summed up for four samples – two samples with  $d_{90} = 14$  and  $6.6 \mu\text{m}$  each treated by  $-0.6$  and  $-0.8$  barg, see **Figure 32** where on vertical axes there is layer thickness in micrometers. All samples had the same suspension loading = 6 g. Layer thickness varies a lot with different particle size – for bigger particles, the thickness is much higher (approx. five times) than for  $6.6 \mu\text{m}$  particles. This means that bigger particles rather create a layer on the wall, instead of filling up the wall (for smaller particles this effect is opposite). Also, for higher vacuum the layer thickness is higher

for both suspensions – for larger particles the difference is 21.7  $\mu\text{m}$  and for smaller ones it is 8.1  $\mu\text{m}$ . However, it has to be noted that for  $d_{90} = 6.6 \mu\text{m}$  the difference is so small that it cannot be considered as a trend. The coating experiments were not repeated in order to verify the small difference.

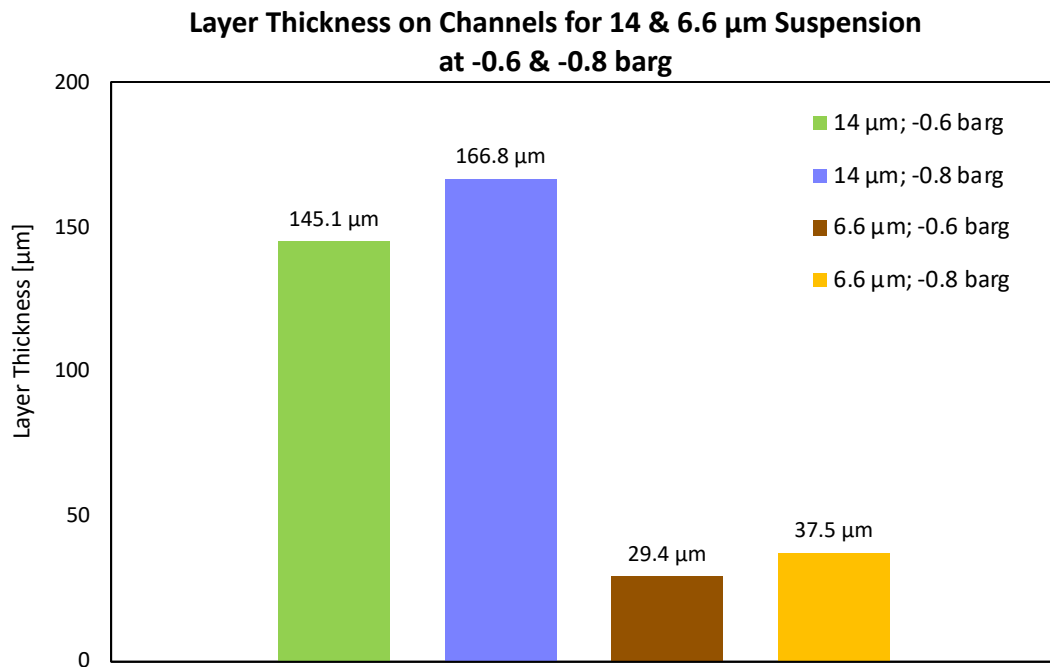


**Figure 32** – Layer thickness on channel of  $d_{90} = 14$  and 6.6  $\mu\text{m}$  for two vacuums:  $-0.6$  and  $-0.8$  barg.

The ratio of on-wall and in-wall coating can also be calculated. The SEM images were segmented – each pixel was allocated to one phase (pore, coating, substrate) only. The number of pixels representing the on-wall or in-wall coating was then divided by the total no. of coating pixels. This operation was also done in the ImageJ software. This is an important value for comparing between coating with different particle size.<sup>24</sup>

Comparison of the on-wall/in-wall ratio is summed up in **Table 7** – two types of particle sizes with various vacuum settings for each of them. Generally, larger particles rather created an on-wall layer while the smaller particles rather penetrated and filled the substrate walls. Also, when higher vacuum is used particles are more contained in the

substrate wall – this trend is same for both particle sizes but it is less significant for smaller particles. Smaller particles almost completely fill substrate walls, see **Figure 34**, and when higher vacuum was used, particles partially created a thin layer on the opposite side of the wall, see **Figure 43** in **Appendix**. The differences between coating in-wall and on-wall for different vacuum sets is not clearly visible in the photos, SEM images for higher vacuum –0.8 barg (**Figure 42** and **Figure 43**) are therefore enclosed in **Appendix**. Also suspension with  $d_{90} = 10 \mu\text{m}$  was used with pressure –0.6 barg and then it was analyzed by the same procedure – particles on the wall were contained in 82.04 % and in wall 17.96 %.

**Table 7** – Comparing coating in- and on-wall of channel for –0.6 and –0.8 barg vacuum with two various particle sizes.

Sample Type	Particles in the Wall [%]	Particles on the Wall [%]
$d_{90} = 14 \mu\text{m};$ <b>–0.6 [barg]</b>	25.40	74.60
$d_{90} = 14 \mu\text{m};$ <b>–0.8 [barg]</b>	28.48	71.52
$d_{90} = 6.6 \mu\text{m};$ <b>–0.6 [barg]</b>	88.70	11.30
$d_{90} = 6.6 \mu\text{m};$ <b>–0.8 [barg]</b>	89.96	10.04

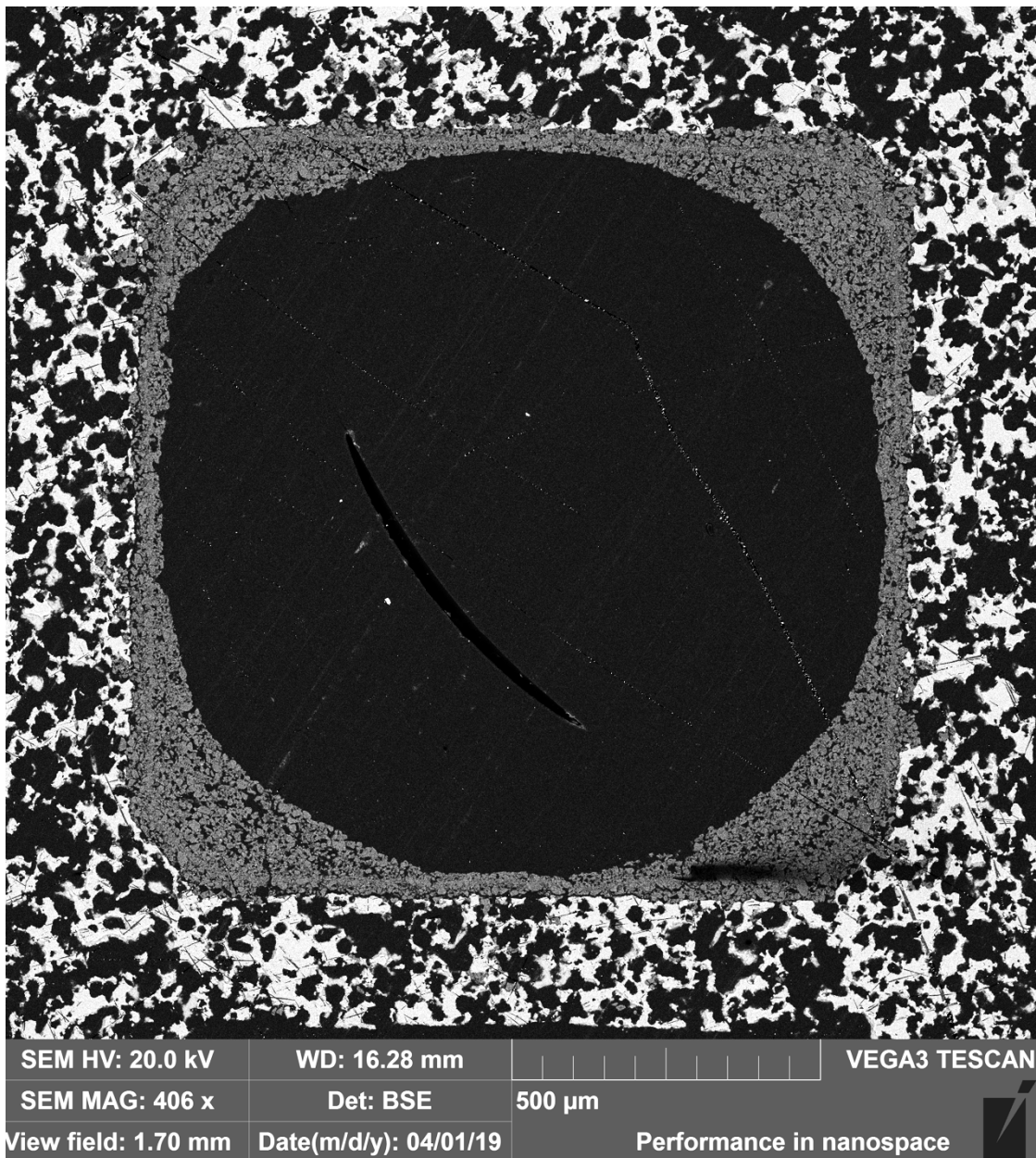
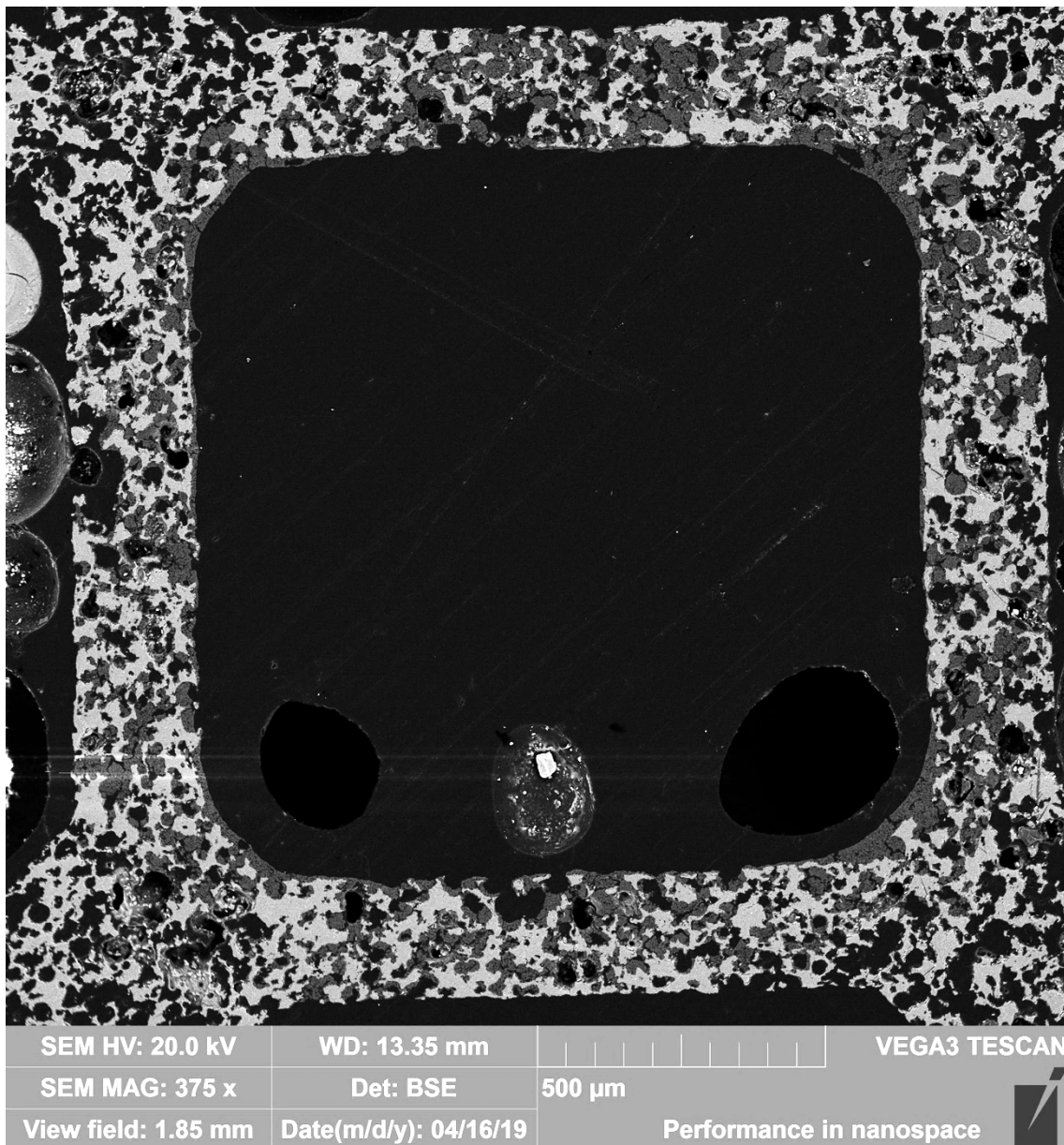


**Figure 33** – SEM micrograph of a single channel from a sample vacuum-coated with a  $d_{90} = 14 \mu\text{m}$  suspension with vacuum  $-0.6 \text{ barg}$ .



SEM HV: 20.0 kV

WD: 13.35 mm

VEGA3 TESCAN

SEM MAG: 375 x

Det: BSE

500  $\mu\text{m}$

View field: 1.85 mm

Date(m/d/y): 04/16/19

Performance in nanospace

**Figure 34** – SEM micrograph of a single channel from a sample vacuum-coated with a  $d_{90} = 6.6 \mu\text{m}$  suspension with vacuum  $-0.6 \text{ barg}$ .

#### 4.2.5 Wet Sample Coating

This type of experiments were focused on comparing the impact of modifying samples before coating procedure, specifically dipping the filter substrates in water. The samples were dipped in distilled water for 1.75 hours. This time was long enough to soak up the water in pores. The next step was to removed excess water by the same vacuum set-up as for coating process – the time was as short as possible to remove water on the substrate surface, not in pores. Then suspension was loaded and the rest of procedure was the same as before (coating by vacuum –0.6 barg, analysis – SEM and ImageJ).

More particles were contained on-wall when compared to dry samples for both particle sizes 14 and 6.6  $\mu\text{m}$ , see **Table 8**. The effect was more apparent for bigger particles – for  $d_{90} = 14 \mu\text{m}$  difference is 11.78 % and for 6.6 it is 5.75 %. The explanation is that pores in the wall were partially filled by water prior to the coating so they could not be filled up by particles.

**Table 8** – Comparing coating in- and on-wall of channel for dry and wet sample for both suspensions.

Sample Type	Particles in the Wall [%]	Particles on the Wall [%]
$d_{90} = 14 [\mu\text{m}]$ ; <b>-0.6 [barg]</b> ; dry	25.40	74.60
$d_{90} = 14 [\mu\text{m}]$ ; <b>-0.6 [barg]</b> ; wet	13.62	86.38
$d_{90} = 6.6 [\mu\text{m}]$ ; <b>-0.6 [barg]</b> ; dry	90.97	11.30
$d_{90} = 6.6 [\mu\text{m}]$ ; <b>-0.6 [barg]</b> ; wet	82.95	17.05

Layer thickness for both suspensions with sample-modifying is shown in **Figure 34**. All samples had the same suspension loading = 6 g. Comparing layer thickness of wet and dry samples is slightly different specially for  $d_{90} = 14 \mu\text{m}$  – the difference is  $39.5 \mu\text{m}$  and for  $d_{90} = 6.6 \mu\text{m}$  it is  $1.8 \mu\text{m}$ . Layers are mainly located on the substrate surface than in-wall for both particle sizes (approximately the half width of the channel wall is filled by  $d_{90} = 6.6 \mu\text{m}$  particles), see **Figure 36** and **Figure 37**. In comparing all results (the ratio in-/on-wall, layer thickness and photos), layers seem to be more on the substrate surface and more compact.

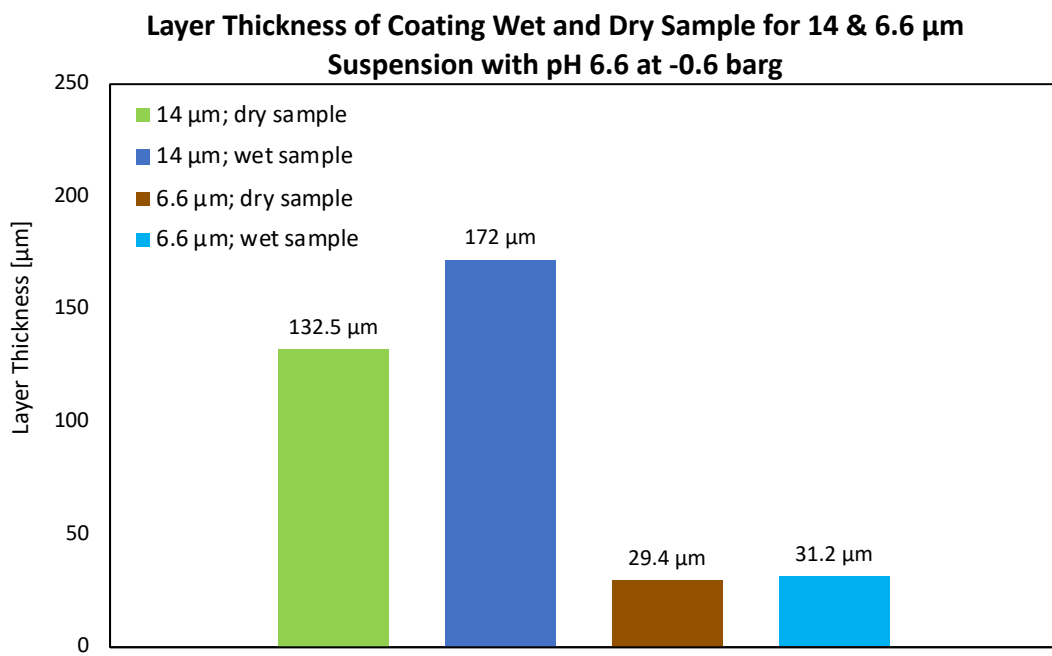


**Figure 35** – Comparing layer thickness of wet and dry sample for particle sizes 14 and  $6.6 \mu\text{m}$  coated by vacuum  $-0.6 \text{ barg}$ .

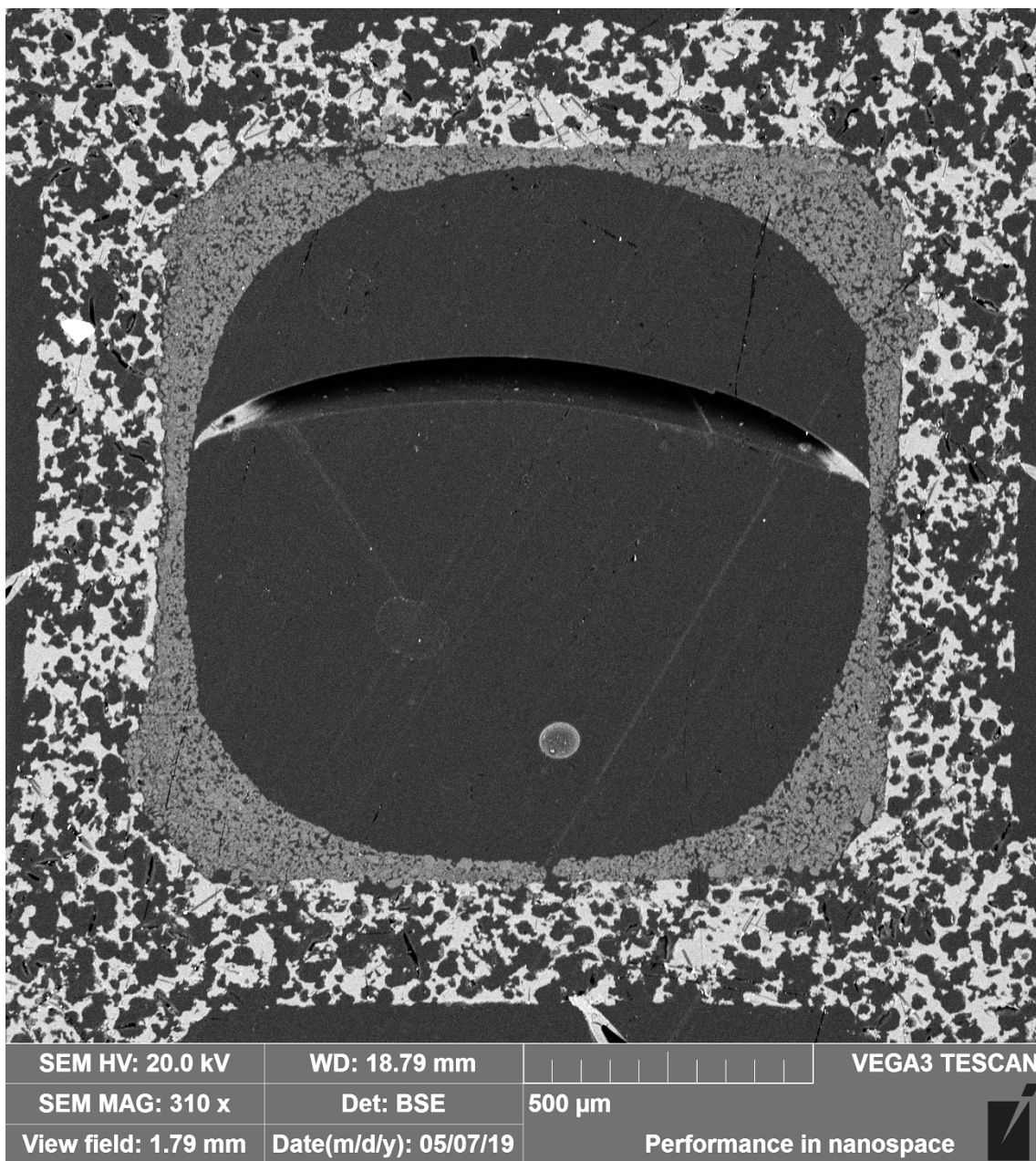


**Figure 36** – SEM micrograph of a single channel from a wet sample vacuum-coated with a  $d_{90} = 14 \mu\text{m}$  suspension with vacuum  $-0.6 \text{ barg}$ .

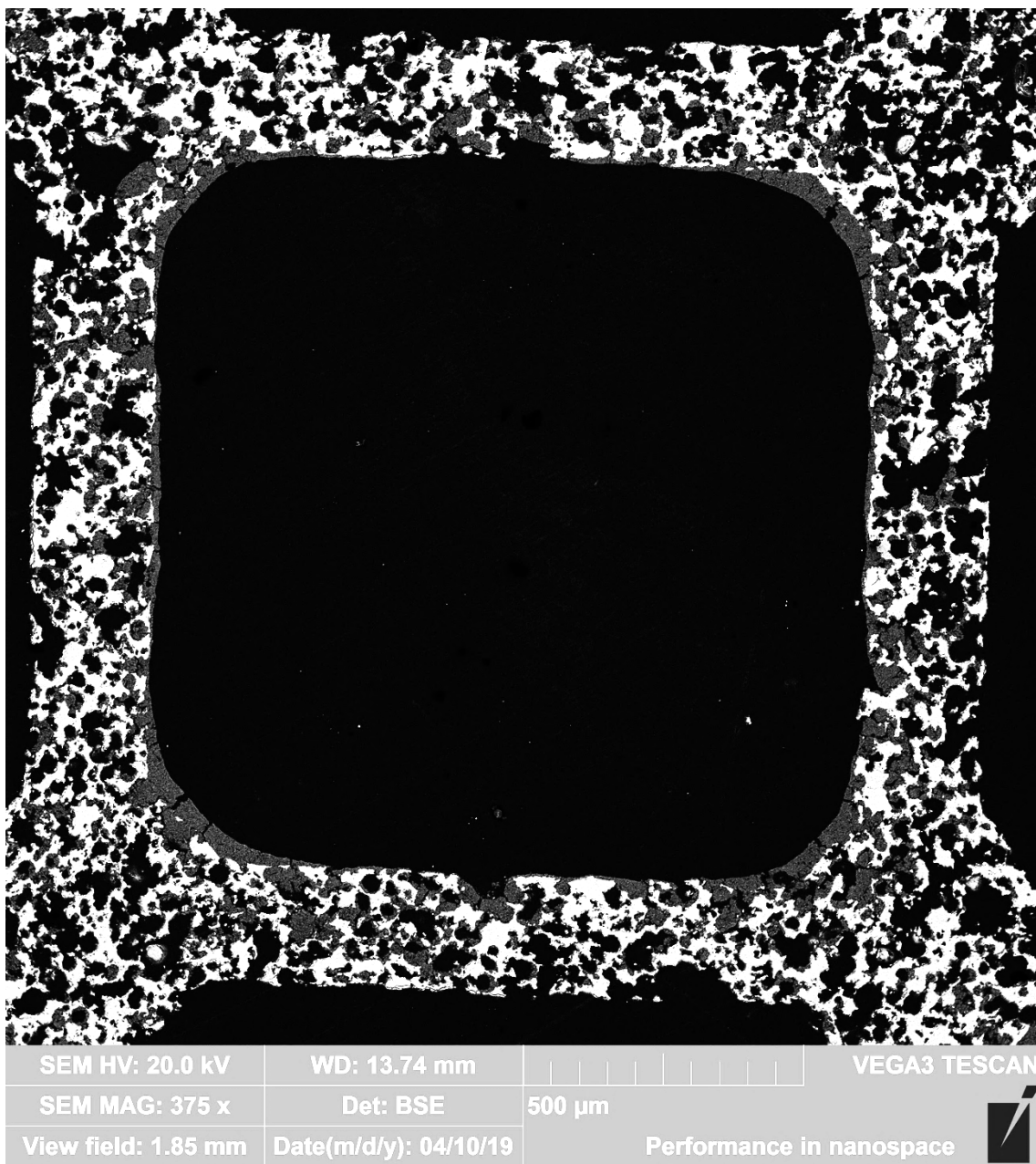


**Figure 37** – SEM micrograph of a single channel from a wet sample vacuum-coated with a  $d_{90} = 6.6 \mu\text{m}$  suspension with vacuum  $-0.6 \text{ barg}$ .

#### 4.2.6 Impact of Sealing During Vacuum Coating

In previously discussed samples, sometimes some side channels were not coated along the sample length at the same distance as the rest of channels – coating layers were not

distributed same along the sample length. To obtain even distribution of coated length in all channels, apparatus was slightly modified by additional sealing between the tube and funnel – it was wrapped by plastic film. Coating length was almost the same as at previous experiments but this time it could be seen that all channels were coated. The samples were not analyzed in detail by SEM and ImageJ.

### 4.3 Testing of Coated Samples

Pressure loss is one of the most important parameters of particulate filters as described in **Literature Review**. When all important parameters affecting the coating were experimentally investigated and the suitable coating procedure was found, samples were vacuum-coated from both sides so their pressure losses could be measured.

Three suspensions were used –  $d_{90} = 6.6, 10$  and  $14 \mu\text{m}$  with  $\text{pH} = 6.6$ . Some parameters were slightly modified in coating procedure – the suspension loading was 10 g, vacuum was set at  $-0.6$  barg for first coating step and for the second coating it was increased to  $-0.8$  barg. The pressure was increased due to higher pressure loss (during the vacuum coating) caused by the first coated layer. Samples were dried in the same way as mentioned above between the first and second coating step. All experiments can be divided to three groups:

- Standard coating procedure;
- Sample were dipped in distilled water for 1.75 hour prior to the first coating step;
- Coating process with additional sealing.

Overview of pressure loss results for the first type of experiments is shown in **Figure 38**. The pressure loss is significantly influenced by particle size – it increased with growing particle size and therefore also with a growing on-wall/in-wall coating ratio.

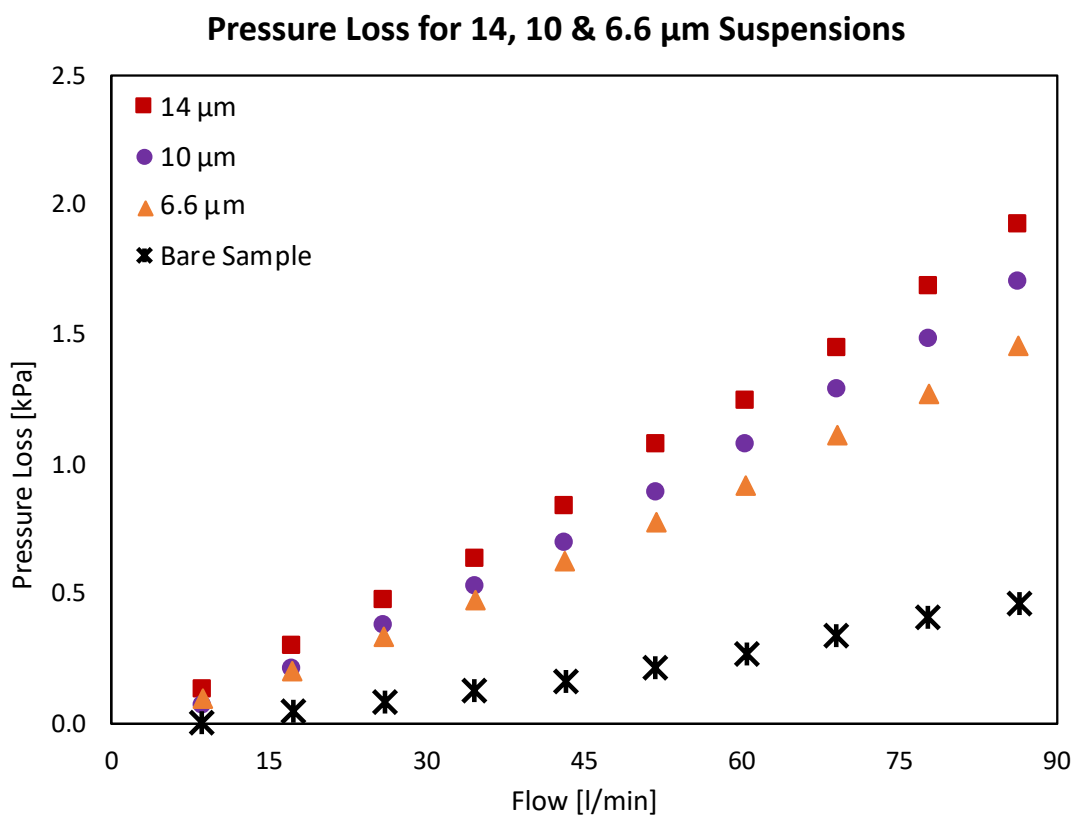


**Figure 38** – Pressure loss measured for samples coated by  $d_{90} = 14, 10$  and  $6.6 \mu\text{m}$  and bare (uncoated) sample.

In the second type of experiments samples were dipped into distilled water for 1.75 hour before the first coating process. Before the second coating procedure samples were not dipped in water to avoid damaging the already coated and re-wetted  $\gamma\text{-Al}_2\text{O}_3$  layer by vacuum. In this case, two types of suspensions were used –  $d_{90} = 14$  and  $6.6 \mu\text{m}$ , see **Figure 39** for bigger particles and **Figure 40** for smaller ones. Pressure loss of wet samples are higher in both examples, which is consistent with the previous findings that more on-wall coating leads to higher pressure loss and wetting the samples results in increased on-wall layer thickness.

In the third category of experiments, the procedure was the same except for the additional sealing as described in **Chapter 4.2.6**. The sealing had the biggest for

$d_{90} = 6.6 \mu\text{m}$  and the smallest for  $10 \mu\text{m}$  particles – see **Figure 40** for the smallest particles and **Figure 45** for  $d_{90} = 10 \mu\text{m}$  (in **Appendix**), for  $14 \mu\text{m}$  see **Figure 39**.

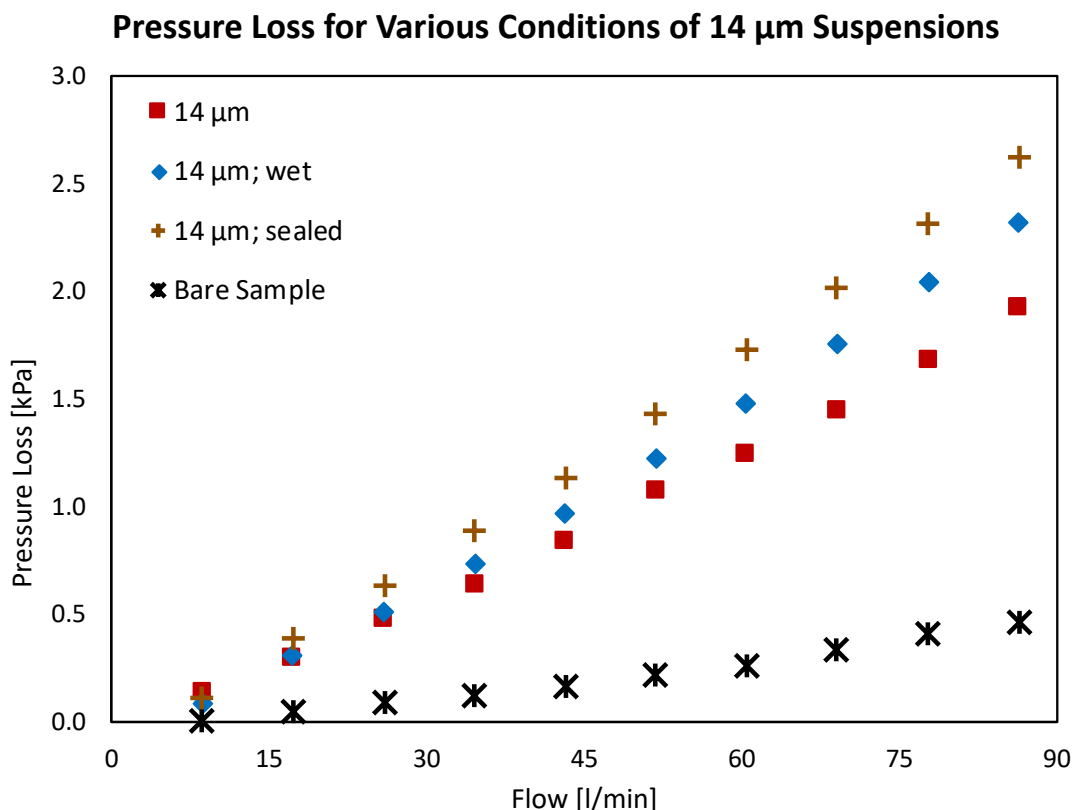


**Figure 39** – Pressure loss for all three modifying coating procedures for  $d_{90} = 14 \mu\text{m}$ .

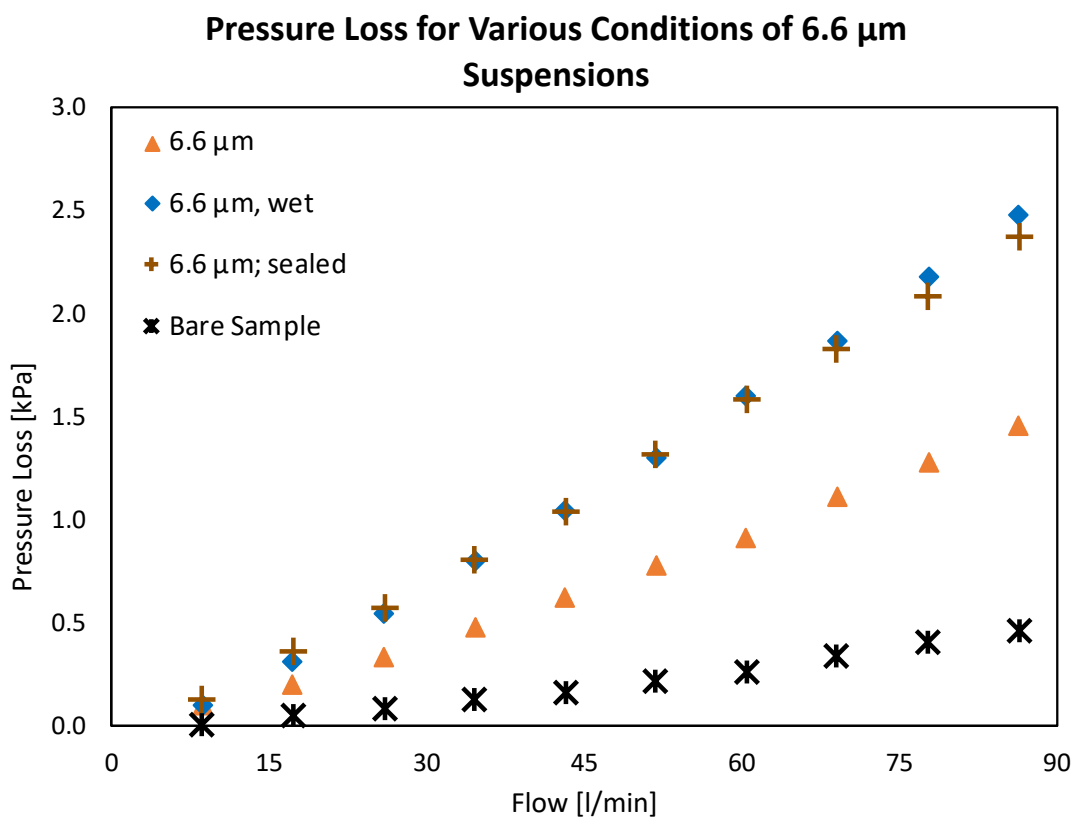


**Figure 40** – Pressure loss for all three modifying coating procedures for  $d_{90} = 6.6 \mu\text{m}$ .

## 5 CONCLUSION

This master thesis was focused on research and development of dip- and vacuum-coating procedures, which were used to coat ceramic monolithic filters.

In the first category of experiments, cuboidal samples were dip-coated by  $\gamma\text{-Al}_2\text{O}_3$  suspension with  $d_{90} = 14 \mu\text{m}$  with different pH 7.3, 6.8 and 6.6, the viscosity decreasing with lowering pH (however, all the suspensions were still in gel-like state when no external force was applied). The longest coated length was obtained for the pH = 6.6 suspension due to its lowest viscosity. This pH was therefore chosen as a standard for the vacuum-coating process; lower pH was tested as well, however, the suspension was no longer in gel-like state and was very difficult to dose.

When the pH effect was tested, cylindrical samples were vacuum-coated to investigate which parameters and how they influence coated length, layer thickness and its uniformity. These parameters were studied: suspension loading, pH, particle sizes, pressure during the vacuum coating and effect of wetting the substrate with water prior to the coating. The aim was to coat at least half of the sample length, which was 11.4 cm. Three suspensions were used with particle sizes  $d_{90} = 14, 10$  and  $6.6 \mu\text{m}$ .

The coated length was clearly affected by suspension loading; the length increased with the loading and for 10 g of suspension, 8.5 cm of channels were coated, comfortably exceeding half of the sample length. Applying higher vacuum ( $-0.8$  instead of  $-0.6$  barg) also slightly increased the coated length (approx. by 0.8 cm). When layer thickness was analyzed, larger particles ( $d_{90} = 14 \mu\text{m}$ ) rather formed a layer on the walls instead of filling them. For smaller particles ( $d_{90} = 6.6 \mu\text{m}$ ) the effect was opposite – most of the particles were inside the walls. The thickness of on-wall layer was slightly higher when higher vacuum was applied and/or the filter substrates were dipped in water prior the coating – part of pores in the walls could not be filled by suspension because they were already filled by water. Furthermore, additional sealing of the apparatus improved the distribution of coating.

When suitable parameters were found, samples were coated from both sides with three types of suspension were used –  $d_{90} = 14$ , 10 and 6.6  $\mu\text{m}$ . Pressure loss of the coated filters was measured for three varied sample modification – samples coated by the standard procedure, pre-wetted samples and samples coated with additional sealing of apparatus. The pressure loss increased with growing particle size and therefore with a growing on-wall/in-wall coating ratio. For the same reason, pre-wetting of the samples resulted in slightly higher pressure loss. Additional sealing led to increase in pressure drop as well due to more evenly distributed coating. The lowest pressure loss (as desired for the industrial application) was achieved while using  $d_{90} = 6.6 \mu\text{m}$  particles. However, it needs to be noted that the pressure loss of an analogous sample, which was prepared with additional apparatus sealing, increased. In the future work, additional studies need to be carried out to study homogeneity of the coating distribution.

## LITERATURE

1. Haagen-Smit, A. J., Chemistry and Physiology of Los Angeles Smog. *Industrial & Engineering Chemistry* **1952**, 44 (6), 1342-1346.
2. Larson, G. P., J.C. Chipman, and E.K. Kaupfr, Study of the Distribution and Effects of Auto Exhaust Gases. *Journal of the Air Pollution Control Association* **1955**, 5 (2), 84-90.
3. Nievergeld, A. J., Automotive Exhaust Gas Conversion: Reaction Kinetics. *University of Technology Eindhoven* **1998**.
4. Twigg, M. V., Roles of catalytic oxidation in control of vehicle exhaust emissions. *Catalysis Today* **2006**, 117 (4), 407-418.
5. Acres, G. J. K.; Harrison, B. J. T. i. C., The Development of Catalysts for Emission Control from Motor Vehicles: Early Research at Johnson Matthey. **2004**, 28 (1), 3-11.
6. Commision, E., European Emission Standards. <https://dieselnet.com/standards/eu/ld.php> **15.03.2018**.
7. Heck, R. M. a. R. J. F., Automotive Exhaust Catalysts. *Applied Catalysis A: General* **2001**, 221 (1), 443-457.
8. Qian, Y.; Li, Z.; Yu, L.; Wang, X.; Lu, X., Review of the state-of-the-art of particulate matter emissions from modern gasoline fueled engines. *Applied Energy* **2019**, 238, 1269-1298.
9. Guan, B.; Zhan, R.; Lin, H.; Huang, Z., Review of the state-of-the-art of exhaust particulate filter technology in internal combustion engines. *Journal of Environmental Management* **2015**, 154, 225-258.
10. Labík, P. Příprava katalytických monolitických reaktorů pro oxidaci výfukových plynů. University of Chemistry and Technology at Prague, Praha, 2018.
11. Heck, R. M. a. R. J. F., *Catalytic Air Pollution Control: Commercial Technology*. 1995.
12. Rouquerol, J., et al., Recommendations for the characterization of porous solids (Technical Report). *International Union of Pure and Applied Chemistry* **1994**, 66 (8), p. 1739-1758.
13. Dudák, M., et al., Prediction of diffusivity and conversion of n-decane and CO in coated Pt/. *Applied Catalysis B: Environmental* **2014**, 150-151, p. 446-458.
14. Blažek, M. Nanášení porézních katalytických vrstev do kanálků monolitického reaktoru. University of Chemistry and Technology at Prague, 2017.
15. Guan, B.; Zhan, R.; Lin, H.; Huang, Z., Review of state of the art technologies of selective catalytic reduction of NOx from diesel engine exhaust. *Applied Thermal Engineering* **2014**, 66 (1), 395-414.
16. Kočí, P., *Průmyslové reaktory - Katalytické reaktory pro ochranu ovzduší*. 2019.
17. Takahashi, N.; Shinjoh, H.; Iijima, T.; Suzuki, T.; Yamazaki, K.; Yokota, K.; Suzuki, H.; Miyoshi, N.; Matsumoto, S.-i.; Tanizawa, T.; Tanaka, T.; Tateishi, S.-s.; Kasahara, K., The new concept 3-way catalyst for automotive lean-burn engine: NOx storage and reduction catalyst. *Catalysis Today* **1996**, 27 (1), 63-69.
18. Chorkendorff, I. a. J. W. N., *Concepts of Modern Catalysis and Kinetics*. John Wiley & Sons: 2003.

19. Twigg, M. V., Progress and future challenges in controlling automotive exhaust gas emissions. *Applied Catalysis B: Environmental* **2007**, *70* (1), 2-15.
20. F. Haas, H. F., Structural Characterization of Automotive Catalysts. *Advanced Engineering Materials* **2005**, *7* (10), 899-913.
21. Farrauto, R. J.; Heck, R. M., Catalytic converters: state of the art and perspectives. *Catalysis Today* **1999**, *51* (3), 351-360.
22. Nunan, J. G.; Robota, H. J.; Cohn, M. J.; Bradley, S. A., Physicochemical properties of Ce-containing three-way catalysts and the effect of Ce on catalyst activity. *Journal of Catalysis* **1992**, *133* (2), 309-324.
23. Three-Way Catalyst. <https://www.jmsec.com/air-pollution-solutions/three-way-catalyst/>.
24. Václavík, M.; Plachá, M.; Kočí, P.; Svoboda, M.; Hotchkiss, T.; Novák, V.; Thompsett, D., Structure characterisation of catalytic particulate filters for automotive exhaust gas aftertreatment. *Materials Characterization* **2017**, *134*, 311-318.
25. Weibel, M.; Waldbüßer, N.; Wunsch, R.; Chatterjee, D.; Bandl-Konrad, B.; Krutzsch, B., A Novel Approach to Catalysis for NOxReduction in Diesel Exhaust Gas. *Topics in Catalysis* **2009**, *52* (13), 1702.
26. Zheng, Y.; Liu, Y.; Harold, M. P.; Luss, D., LNT-SCR dual-layer catalysts optimized for lean NOx reduction by H2 and CO. *Applied Catalysis B: Environmental* **2014**, *148-149*, 311-321.
27. Václavík, M.; Novák, V.; Březina, J.; Kočí, P.; Gregori, G.; Thompsett, D., Effect of diffusion limitation on the performance of multi-layer oxidation and lean NOx trap catalysts. *Catalysis Today* **2016**, *273*, 112-120.
28. Koltsakis, G.; Haralampous, O.; Depcik, C.; Ragone, J. C., Catalyzed diesel particulate filter modeling. In *Reviews in Chemical Engineering*, 2013; Vol. 29, p 1.
29. Schejbal, M.; Štěpánek, J.; Marek, M.; Kočí, P.; Kubíček, M., Modelling of soot oxidation by NO2 in various types of diesel particulate filters. *Fuel* **2010**, *89* (9), 2365-2375.
30. Reid, N., What Diesel Drivers Need to Know About Their DPF. <http://blog.greenflag.com/2014/diesel-drivers-need-know-dpf/> **09-29-2014**.
31. Aravelli, K., Heibel, A, Improved Lifetime Pressure Drop Management for Robust Cordierite (RC) Filters with Asymmetric Cell Technology (ACT). *SAE Technical Paper* **2007**, *1*.
32. Seo, J. M., Park, W.S., Lee, M.J., The Best Choice of Gasoline/diesel Particulate Filter to Meet Future Particulate Matter Regulation. *SAE Technical Paper* **2012**, *01*.
33. Bardon, S., Bouteiller, B., Bonnail, N., Girot, P., Gleize, V., Oxarango, L., Higelin, P., Michelin, J., Schuerholz, S., Terres, F, Asymmetrical Channels to Increase DPF Lifetime. *SAE Technical Paper* **2004**, *01*.
34. Briot, A., Carranza, F., Girot, P., Bardon, S., Minimizing Filter Volume by Design Optimization. *SAE Technical Paper* **2007**, *1*.
35. Cumaranatunge, L., Chiffey, A., McGonigle, K., Ripley, G., Stetina, J., Lee, A., Storms, C., Kucheruk, D., Sukumar, B., Naseri, M., A study of the soot burning

- efficiency of an SCRF® catalyst vs a CSF during active regeneration events. In *CLEERS*, Johnson Matthey: 2016.
- 36. Joshi, A., Timothy, J. V., Gasoline Particulate Filters—a Review. *Emission Control Science and Technology* **2018**, 4, p. 219-239.
  - 37. Umicore, Catalysed Gasoline Particulate Filter (cGPF). <https://ac.umincore.com/en/technologies/gasoline-particulate-filter/>.
  - 38. Meille, V., Review on methods to deposit catalysts on structured surfaces. *Applied Catalysis A: General* **2006**, 315, 1-17.
  - 39. Avila, P.; Montes, M.; Miró, E. E., Monolithic reactors for environmental applications: A review on preparation technologies. *Chemical Engineering Journal* **2005**, 109 (1), 11-36.
  - 40. PURALOX/CATALOX, High Purity Activated Aluminas. [www.sasol.com](http://www.sasol.com) **2005**.
  - 41. Johnson, M. F. L., Surface Area Stability of Aluminas. *Journal of Catalysis* **1990**, 123 (1), 245-259.
  - 42. Macedo, M. I., C.C. Osawa, and C.A. Bertran, Sol-gel Synthesis of Transparent Alumina Gel and Pure Gamma Alumina by Urea Hydrolysis of Alumina Nitrate. *Journal of Sol-Gel Science and Technology* **2004**, 30 (3), 135-140.
  - 43. Trueba, M.; Trasatti, S. P.,  $\gamma$ -Alumina as a Support for Catalysts: A Review of Fundamental Aspects. **2005**, 2005 (17), 3393-3403.
  - 44. Chang, J. C.; Lange, F. F.; Pearson, D. S.; Pollinger, J. P., Pressure Sensitivity for Particle Packing of Aqueous Al<sub>2</sub>O<sub>3</sub> Slurries vs Interparticle Potential. **1994**, 77 (5), 1357-1360.
  - 45. Rawle, A., Basic of principles of particle-size analysis. *Surface Coatings International Part A: Coatings Journal* **2003**, 86 (2), 58-65.

## LIST OF ABBREVIATIONS

ACT	Asymmetric Cell Technology
ASC	Ammonia Slip Catalyst
BET	Brunauer-Emmett-Teller adsorption theory
BSE	Backscattered Electrons
cGPF	catalyzed Gasoline Particulate Filter
CSF	Catalyzed Soot Filter
CVD	Chemical Vapor Deposition
DEF	Diesel Exhaust Fluid
deNO <sub>x</sub>	NO <sub>x</sub> reduction technology
DOC	Diesel Oxidation Catalyst
DPF	Diesel Particulate Filter
EES	Euro Emissions Standard
GDI	gasoline direct injection
GPF	Gasoline Particulate Filter
HC	hydrocarbons
IUPAC	International Union of Pure and Applied Chemistry
LNT	Lean NO <sub>x</sub> Trap
L.O.I.	loss on ignition
MFC	Mass Flow Controller
NSCR NO <sub>x</sub>	Storage and Reduction Catalyst
NSRC NO <sub>x</sub>	Storage and Reduction Catalyst
PAH(s)	Polycyclic Aromatic Hydrocarbons
PFI	port fuel injection
PLA	polylactic acid
PM	particulate matter
PSD	particle size distribution
PTFE	polytetrafluorethylen
TE	Transmission Electrons
TWC	Three-Way Catalyst
SCR	Selective Catalytic Reduction
SCRF	Selective Catalytic Reduction Filter
SE	Secondary Electrons
SEM	Scanning Electron Microscope
SOF	soluble organic fraction
SE	Secondary Electrons

## LIST OF SYMBOLS

$d_{10}$	quantile 10 % of PSD	[μm]
$d_{50}$	quantile 50 % of PSD	[μm]
$d_{90}$	quantile 90 % of PSD	[μm]
pH	potential of hydrogen	[–]
$\gamma$	crystalline modification of aluminum oxide	[–]
$\lambda$	fuel-air molar ration	[–]

## **LIST OF TABLES**

<b>Table 1</b> – Development of European Emission Standard for passenger automobiles (category M1). <sup>6</sup> .....	3
<b>Table 2</b> – Example of real exhaust gases composition. <sup>7</sup> .....	4
<b>Table 3</b> – SCFa140 all characteristics. <sup>40</sup> .....	22
<b>Table 4</b> – Description of mill set up and suspension parameters.....	23
<b>Table 5</b> – The overview of all parameters of used suspensions.....	26
<b>Table 6</b> – Overview of dip-coating steps of cuboidal samples. ....	28
<b>Table 7</b> – Comparing coating in- and on-wall of channel for $-0.6$ and $-0.8$ barg vacuum with two various particle sizes. ....	45
<b>Table 8</b> – Comparing coating in- and on-wall of channel for dry and wet sample for both suspensions. ....	48

## LIST OF FIGURES

<b>Figure 1</b> – Development of particulate matter from fuel. <sup>8</sup> .....	7
<b>Figure 2</b> – Catalytic converter of monolithic type. <sup>14</sup> .....	9
<b>Figure 3</b> – Operating Window. <sup>23</sup> .....	12
<b>Figure 4</b> – The sketch of wall-flow monolithic particulate matter filter. <sup>24</sup> .....	13
<b>Figure 5</b> – Regeneration cycle of particulate filter. <sup>30</sup> .....	14
<b>Figure 6</b> – Standard and Asymmetric Cell Technology channels comparing with loaded soot. <sup>31</sup> .....	15
<b>Figure 7</b> – Schematic description of standard square cell and “wavy” cell geometry of honeycomb structures. <sup>34</sup> .....	15
<b>Figure 8</b> – Arrangement with CSF of exhaust gas-treatment used for Diesel engines. <sup>35</sup> .....	16
<b>Figure 9</b> – Arrangement with SCRF of exhaust gas-treatment used for Diesel engines. <sup>35</sup> .....	17
<b>Figure 10</b> – TWC with cGPF at various arrangement. <sup>37</sup> .....	18
<b>Figure 11</b> – Dip-coating method. <sup>14</sup> .....	20
<b>Figure 12</b> – The sketch of sample preparation with all steps, important parameters and components. ....	21
<b>Figure 13</b> – Dependence of volume particles size on milling time determined by $d_{90}$ , $d_{50}$ and $d_{10}$ . ....	24
<b>Figure 14</b> – Volume particle size distribution of all used suspensions.....	25
<b>Figure 15</b> – The sketch of cuboidal samples with sizes.....	27
<b>Figure 16</b> – Scheme of blown device and direction paths. ....	28
<b>Figure 17</b> – The sketch of cylindrical samples with sizes. ....	29
<b>Figure 18</b> – The lay-out of the tube from cut- and vertical projection with all sizes....	30
<b>Figure 19</b> – The lay-out of the funnel from cut-projection with all sizes and printed and assembled apparatus with vacuum system.....	31
<b>Figure 20</b> – Scheme of vacuum coating apparatus. ....	32
<b>Figure 21</b> – Sketch of pressure loss measurement. ....	32
<b>Figure 22</b> – Photo of sealed sample prior to the pressure drop measurement. ....	33

<b>Figure 23</b> – Cut cylindric sample to investigate coated length (sample coated by $d_{90} = 14 \mu\text{m}$ suspension). Almost all inlet channels are coated – the layer is clearly visible.	34
<b>Figure 24</b> – Comparing dynamic viscosity of suspensions with pH = 7.3, 6.8 and 6.6 for the $d_{90} = 14 \mu\text{m}$ suspension.....	36
<b>Figure 25</b> – Comparing coated length of $d_{90} = 14 \mu\text{m}$ suspension with various pH for dip-coated cuboidal samples.....	36
<b>Figure 26</b> – SEM micrograph of a single channel from a sample dip-coated with a $d_{90} = 14 \mu\text{m}$ suspension with pH = 6.6.....	37
<b>Figure 27</b> – Dependency of coated length on suspension loading on for $d_{90} = 10 \mu\text{m}$ .	39
<b>Figure 28</b> – Suspension $d_{90} = 14 \mu\text{m}$ coating with various pH.....	40
<b>Figure 29</b> – Suspension $d_{90} = 6.6 \mu\text{m}$ coating with various pH.....	41
<b>Figure 30</b> – Coated length of various pressures set for the vacuum coating of $d_{90} = 14 \mu\text{m}$ suspension.....	42
<b>Figure 31</b> – Coated length of various pressures set for the vacuum coating of $d_{90} = 6.6 \mu\text{m}$ suspension. ....	43
<b>Figure 32</b> – Layer thickness on channel of $d_{90} = 14$ and $6.6 \mu\text{m}$ for two vacuums: $-0.6$ and $-0.8 \text{ barg}$ .....	44
<b>Figure 33</b> – SEM micrograph of a single channel from a sample vacuum-coated with a $d_{90} = 14 \mu\text{m}$ suspension with vacuum $-0.6 \text{ barg}$ .....	46
<b>Figure 34</b> – SEM micrograph of a single channel from a sample vacuum-coated with a $d_{90} = 6.6 \mu\text{m}$ suspension with vacuum $-0.6 \text{ barg}$ .....	47
<b>Figure 35</b> – Comparing layer thickness of wet and dry sample for particle sizes 14 and $6.6 \mu\text{m}$ coated by vacuum $-0.6 \text{ barg}$ .....	49
<b>Figure 36</b> – SEM micrograph of a single channel from a wet sample vacuum-coated with a $d_{90} = 14 \mu\text{m}$ suspension with vacuum $-0.6 \text{ barg}$ .....	50
<b>Figure 37</b> – SEM micrograph of a single channel from a wet sample vacuum-coated with a $d_{90} = 6.6 \mu\text{m}$ suspension with vacuum $-0.6 \text{ barg}$ .....	51
<b>Figure 38</b> – Pressure loss measured for samples coated by $d_{90} = 14$ , 10 and $6.6 \mu\text{m}$ and bare (uncoated) sample. ....	53
<b>Figure 39</b> – Pressure loss for all three modifying coating procedures for $d_{90} = 14 \mu\text{m}$ . ....	54

<b>Figure 40</b> – Pressure loss for all three modifying coating procedures for $d_{90} = 6.6 \mu\text{m}$ .	55
<b>Figure 41</b> – Dynamic viscosity of $d_{90} = 14, 10$ and $6.6 \mu\text{m}$ suspension with various pH.	67
<b>Figure 42</b> – SEM micrograph of a single channel from a sample vacuum-coated with a $d_{90} = 14 \mu\text{m}$ suspension with vacuum $-0.8 \text{ barg}$	68
<b>Figure 43</b> – SEM micrograph of a single channel from a sample vacuum-coated with a $d_{90} = 6.6 \mu\text{m}$ suspension with vacuum $-0.8 \text{ barg}$	69
<b>Figure 44</b> – Comparing pressure loss for wet and dry samples for $d_{90} = 14$ and $6.6 \mu\text{m}$ particles	70
<b>Figure 45</b> – Pressure loss for two conditions (normal and sealing) of coating procedure for $d_{90} = 10 \mu\text{m}$ .	71

## APPENDIX

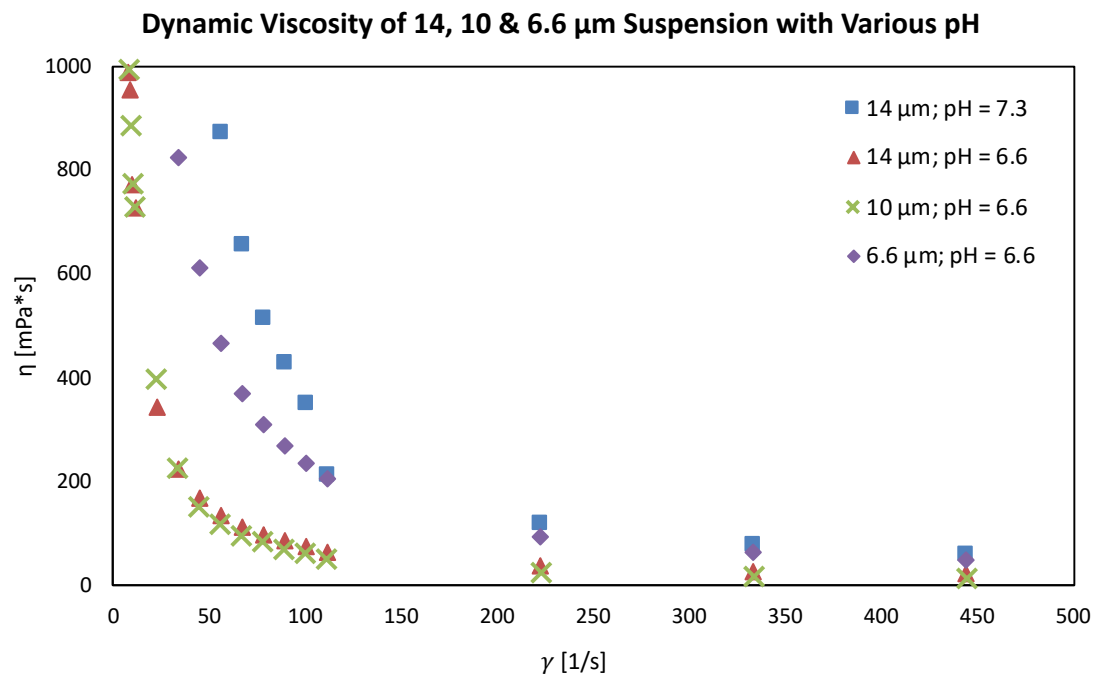


**Figure 41** – Dynamic viscosity of  $d_{90} = 14, 10$  and  $6.6 \mu\text{m}$  suspension with various pH.

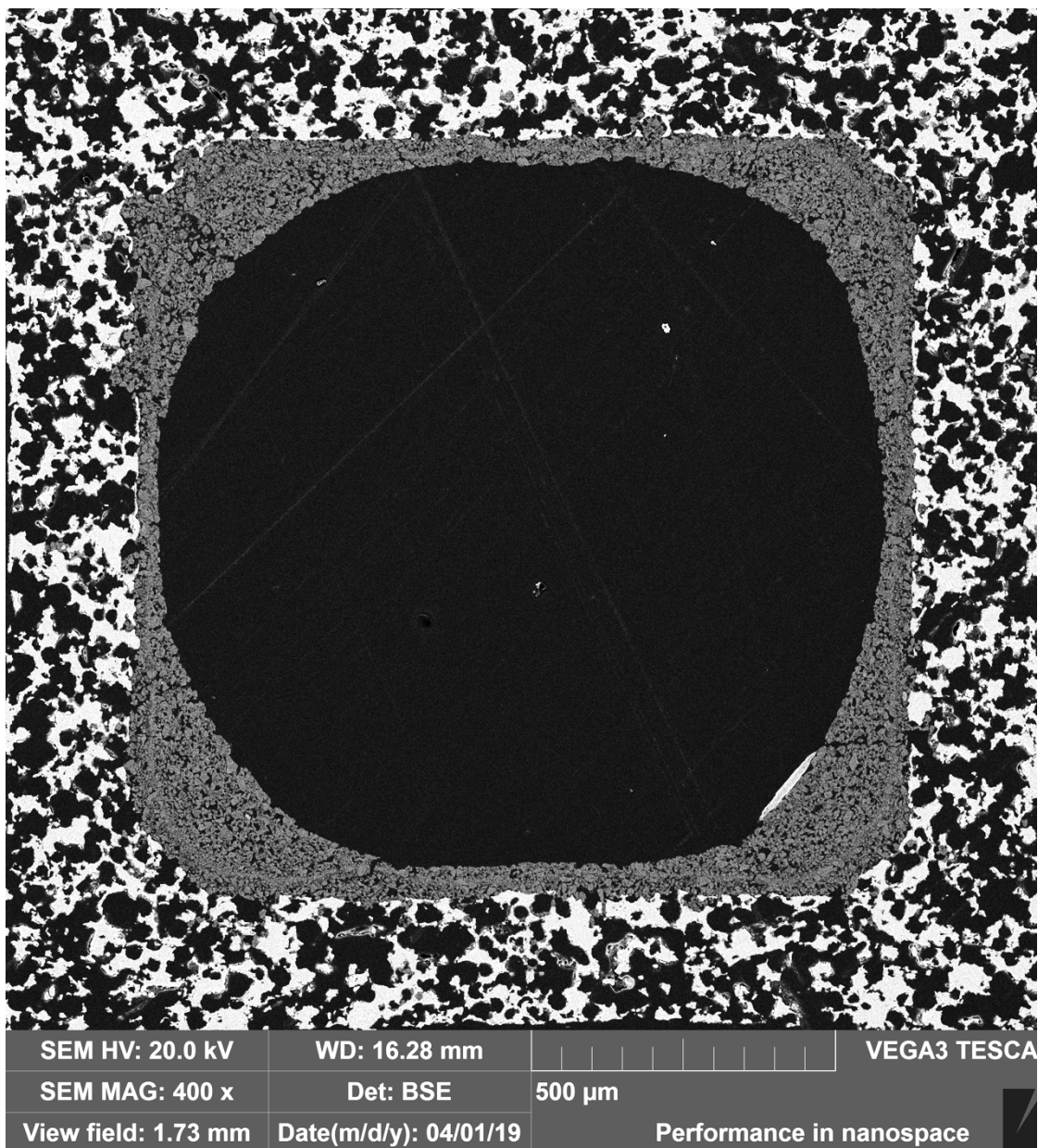


**Figure 42** – SEM micrograph of a single channel from a sample vacuum-coated with a  $d_{90} = 14 \mu\text{m}$  suspension with vacuum  $-0.8 \text{ barg}$ .

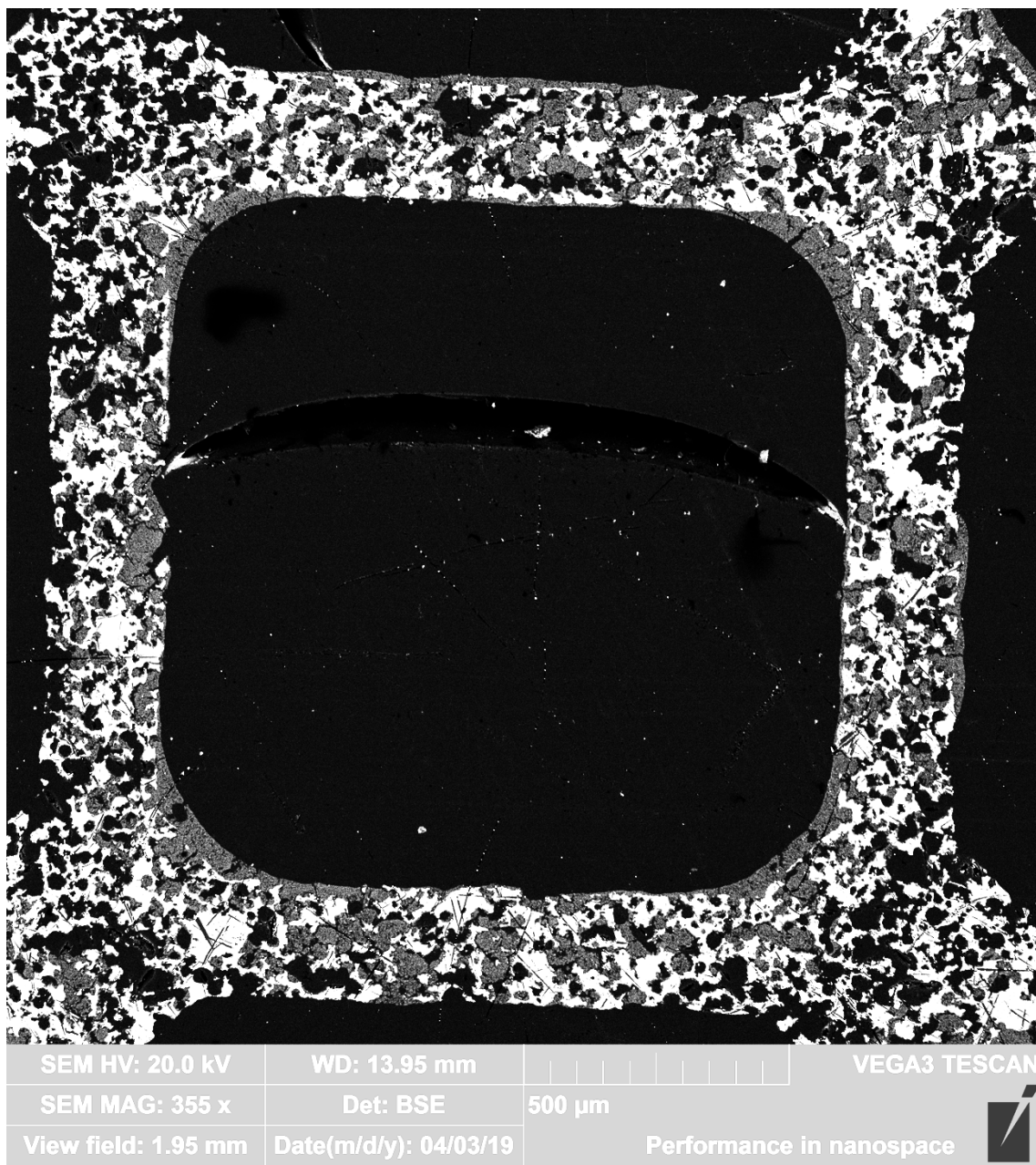


**Figure 43** – SEM micrograph of a single channel from a sample vacuum-coated with a  $d_{90} = 6.6 \mu\text{m}$  suspension with vacuum  $-0.8 \text{ barg}$ .

### Comparing Pressure Loss for Wet & Dry Samples for 14 & 6.6 $\mu\text{m}$ Particles

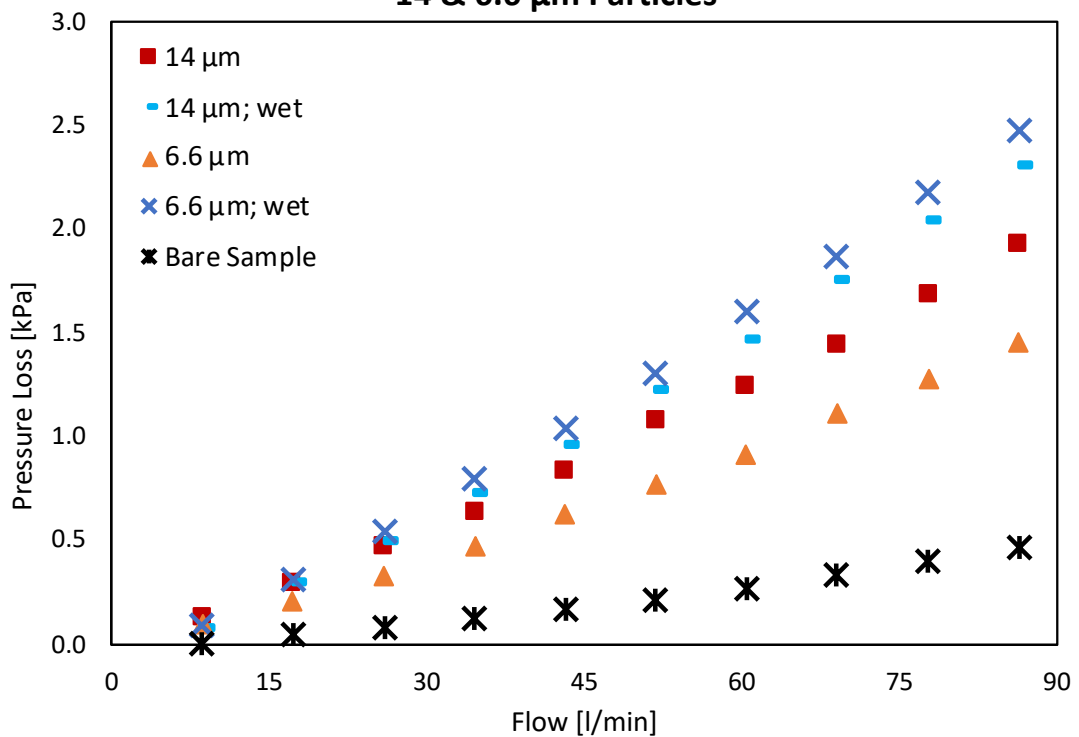


**Figure 44** – Comparing pressure loss for wet and dry samples for  $d_{90} = 14$  and 6.6  $\mu\text{m}$  particles.

### Pressure Loss for Various Conditions of 10 $\mu\text{m}$ Suspensions

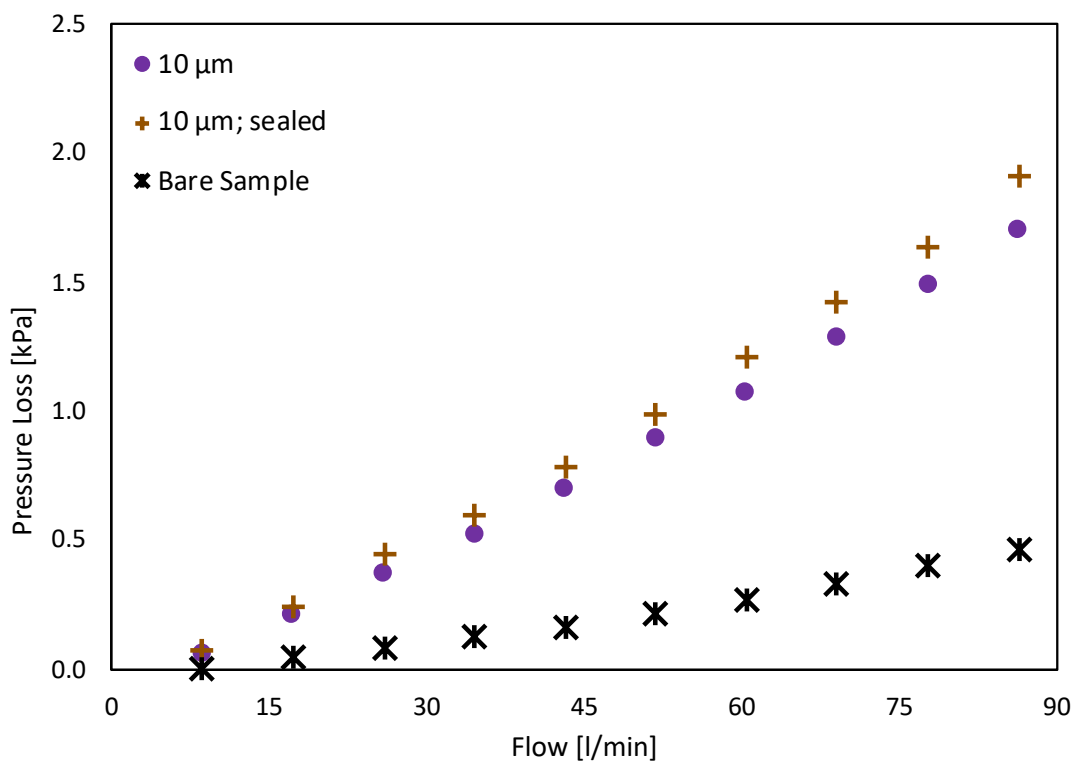


**Figure 45** – Pressure loss for two conditions (normal and sealing) of coating procedure for  $d_{90} = 10 \mu\text{m}$ .